The Astrophysical Journal Supplement Series, 218:26 (20pp), 2015 June doi:10.1088/0067-0049/218/2/26

CHARACTERIZING THE COOL KOIs. VIII. PARAMETERS OF THE PLANETS ORBITING *KEPLER*'S COOLEST DWARFS

Jonathan J. Swift[1,5], Benjamin T. Montet[1,2], Andrew Vanderburg[2], Timothy Morton[3], Philip S. Muirhead[4], and John Asher Johnson[2]

[1] California Institute of Technology, 1200 East California Boulevard, Pasadena, CA 91125, USA
[2] Harvard-Smithsonian Center for Astrophysics, Cambridge, MA 02138, USA
[3] Department of Astrophysical Sciences, Princeton University, 4 Ivy Lane, Peyton Hall, Princeton, NJ 08544, USA
[4] Department of Astronomy, Boston University, 725 Commonwealth Avenue, Boston, MA 02215, USA
Received 2014 December 26; accepted 2015 February 26; published 2015 June 22

ABSTRACT

The coolest dwarf stars targeted by the *Kepler* Mission constitute a relatively small but scientifically valuable subset of the *Kepler* target stars, and provide a high-fidelity, nearby sample of transiting planetary systems. Using archival *Kepler* data spanning the entire primary mission, we perform a uniform analysis to extract, confirm, and characterize the transit signals discovered by the *Kepler* pipeline toward M-type dwarf stars. We recover all but two of the signals reported in a recent listing from the Exoplanet Archive resulting in 163 planet candidates associated with a sample of 104 low-mass stars. We fitted the observed light curves to transit models using a Markov Chain Monte Carlo method and we have made the posterior samples publicly available to facilitate further studies. We fitted empirical transit times to individual transit signals with significantly non-linear ephemerides for accurate recovery of transit parameters and precise measuring of transit timing variations. We also provide the physical parameters for the stellar sample, including new measurements of stellar rotation, allowing the conversion of transit parameters into planet radii and orbital parameters.

Key words: methods: statistical – planets and satellites: general – stars: late-type – stars: low-mass

Supporting material: figure sets, FITS file

1. INTRODUCTION

NASA's *Kepler* Space Mission was designed to monitor more than 150,000 stars within a single 115 square degree patch of sky in search of periodic diminutions of light caused by transiting exoplanets (Borucki et al. 2010; Jenkins et al. 2010; Koch et al. 2010). *Kepler*'s great success in discovering transiting exoplanets (Borucki et al. 2011a, 2011b; Batalha et al. 2013; Burke et al. 2014) has revealed that planets are at least as numerous as stars in the Galaxy (Dressing & Charbonneau 2013; Fressin et al. 2013; Petigura et al. 2013a; Swift et al. 2013; Morton & Swift 2014). Beyond the sheer number of planets, *Kepler* has also provided important insights into the characteristics of the transiting planet population. The multi-transit systems reveal highly coplanar multi-planet systems (Lissauer et al. 2011b; Fang & Margot 2012; Tremaine & Dong 2012; Ballard & Johnson 2014; Fabrycky et al. 2014), many of which are in compact configurations (e.g., Lissauer et al. 2011a; Muirhead et al. 2012b; Swift et al. 2013). The period ratios of adjacent transiting planets show an excess just outside of mean motion resonance (Lissauer et al. 2011b; Fabrycky et al. 2014) that may reflect the mechanisms through which these systems formed (Rein 2012; Goldreich & Schlichting 2014), or else may indicate subsequent evolution of these systems (Lithwick & Wu 2012; Batygin & Morbidelli 2013). The typical surface density profile of the protoplanetary disks from which these planets formed can be estimated using the *Kepler* sample, and implies that either protoplanetary disks contain a large amount of material within ~0.1 AU of the host star (Hansen & Murray 2012; Chiang & Laughlin 2013) or that the planets migrated from their birth places further out in the disk (Swift et al. 2013; Schlichting 2014). Another clue regarding the formation mechanisms behind the *Kepler* planet sample is the radius function—the frequency of planets as a function of their size—which shows unambiguously that there are many more planets with radii smaller than that of Neptune than there are larger ones (Howard et al. 2012; Fressin et al. 2013; Petigura et al. 2013b; Morton & Swift 2014; Foreman-Mackey et al. 2014).

Although the vast majority of *Kepler* target stars are Sun-like ($0.8\,M_\odot \lesssim M_\star \lesssim 1.2\,M_\odot$), several M-type dwarf stars (M dwarfs) have been monitored by *Kepler* over the course of the primary mission. The initial photometric characterization of the M dwarfs in the *Kepler* field was known to be inaccurate because the *Kepler* Input Catalog (KIC) was optimized for Sun-like stars (Brown et al. 2011). However, there have been several efforts to revise the stellar parameters for this sample (e.g., Mann et al. 2012, 2013; Muirhead et al. 2012b, 2014; Dressing & Charbonneau 2013; Newton et al. 2014). Since the physical parameters of a transiting planet are dependent on the stellar parameters, many exciting results have come from a careful examination of this stellar sample (e.g., Johnson et al. 2011a, 2012; Muirhead et al. 2012a, 2013). The depth of a transit signal is proportional to the square of the relative planet radius, $\delta \propto (R_p/R_\star)^2$, allowing the detection of smaller planets around these smaller stars. This higher sensitivity to smaller planets allows the planet population around *Kepler*'s M dwarfs to be well-sampled down to $\lesssim 1 R_\oplus$, where planets are most prevalent (Morton & Swift 2014). Furthermore, the theoretical "habitable zone," in which planets have equilibrium temperatures comparable to that of the Earth, is much closer to these cool, faint stars. This increases the transit probability and number of transits per an observing time baseline, thereby allowing the first detection and measurement of the occurrence

[5] Current address: The Thacher School, 5025 Thacher Road, Ojai, CA 93023, USA.

of Earth-sized planets in the habitable zones of stars (Dressing & Charbonneau 2013; Quintana et al. 2014)

As a supplement to our recent efforts to characterize the lowest mass stars in the *Kepler* field (Muirhead et al. 2012a, 2014), here we focus on the transit signals in the list of M dwarf *Kepler* Objects of Interest (KOIs). The following is a uniform treatment of the sample which we use to derive a statistically useful body of information regarding the properties of the planets orbiting *Kepler*'s lowest-mass stars. In Section 2, we introduce the criteria that were used to define our sample, and in Section 3 we follow with a description of the *Kepler* data products and the preparation of these data for our following analyses. In Section 4, we outline in detail our treatment of the *Kepler* data including a preliminary characterization of the data with outlier rejection and a Markov Chain Monte Carlo parameter estimation. Also in this section, we search for transit timing variations (TTVs) in the light curve data that may be due to mutual gravitational interactions within multi-planet systems or other effects, and perform custom fits to the transit shapes of those sources with significantly non-linear ephemerides. We present the full ensemble of transit candidates and stellar parameters in Section 6 and conclude in Section 7.

2. SAMPLE OF PLANET CANDIDATES

Our list of cool planet host stars is drawn from a recent KOI list available through the Exoplanet Archive (Akeson et al. 2013, downloaded on 2014 September 18) which included the planet candidate sample derived from quarters 1 through 12 of the *Kepler* Mission (Rowe et al. 2015). A total of 4228 planet transit signals toward 3250 targets were selected from the KOI list with dispositions of either "candidate" or "confirmed," comprising a high-fidelity catalog of exoplanets (see, e.g., Morton & Johnson 2011; Morton 2012; Fressin et al. 2013). From this list of candidates, we choose those with host star color K_p–$J > 2$ and $K_p > 14$ as a cut for M dwarfs (Mann et al. 2012). We also include six stars with $r - J > 2.0$ from the study by Muirhead et al. (2014) which pass our red criterion but not our faint criterion: KOI-314, KOI-641, KOI-1725, KOI-3444, KOI-3497, and KOI-4252. Finally, we also include the new planet discovered by Muirhead et al. (2015), KOI-2704.03, or *Kepler*-445d.

We cross-match this full list with the list presented by Muirhead et al. (2014) in which near-infrared spectra for 106 stars toward 103 KOIs are presented. Two of the sources in that list are now categorized as false positives: KOI-1459 and KOI-3090. Another binary system, KOI-4463, consists of stars that appear earlier than M0 in Muirhead et al. (2014), and the KOI is not included in the Dressing & Charbonneau (2013) catalog. We leave these three targets off our list. We also exclude from further consideration a known M dwarf/white dwarf binary in the list (KOI-256 Muirhead et al. 2013), and the giant star KOI-977 (Muirhead et al. 2014). Lastly, we leave of KOI-1686.01 and KOI-1408.02 due to inadequate signal retrieval (see Section 3.2). We therefore consider 97 cool KOIs from the Muirhead et al. (2014) list incorporating all 64 targets in the KOI catalog of Dressing & Charbonneau (2013), save one other now-known false positive, KOI-1164.

The newest release of KOIs (Mullally et al. 2015) postdates both the Muirhead et al. (2014) and Dressing & Charbonneau (2013) catalogs, and so we also cross matched our KOI list against the full catalog of Dressing & Charbonneau (2013) to find seven additional cool stars with candidate transit signals: KOI-2480, KOI-2793 KOI-3102, KOI-3094, KOI-5228, KOI-5359, and KOI-5692. These targets are some of the smallest and longest-period planet candidates in our list and offer exciting possibilities for follow-up observations. We note that our target list is not comprehensive as there are many other independent searches for planet signals in the *Kepler* data (e.g., Fischer et al. 2012; Ofir & Dreizler 2013; Sanchis 2014) and efforts are ongoing.

The final sample we consider for further characterization consists of 163 planet signals toward 104 cool stars observed by *Kepler*. A majority of the stars in this sample (74) show single transit signals, while we find 12 double systems, 10 triple systems, 5 quadruple systems, and 3 quintuple systems. However, the majority of planet candidates, 54.6%, are in multi-transiting systems. The multi-planet systems have a higher probability of being true planetary systems due to a paucity of astrophysical false positive scenarios that could produce multiple, independent transit-like signals within a single *Kepler* aperture (e.g., Lissauer et al. 2014; Rowe et al. 2014) while also passing the data validation pipeline (Wu et al. 2010).

3. DATA PREPARATION

3.1. Kepler Data

The targets in our sample were observed over the entire course of the *Kepler* mission. However, in Quarter 0 only three cool KOI targets were observed. Over the rest of the mission, an average of 87% of the targets in our sample were observed each quarter producing an average of 53,366 long cadence data per target and a total of 5.6 million long cadence photometric measurements for our sample. None of the targets in our sample were observed in short cadence mode until quarter 6 when 9.6% of the targets made the short cadence target list. This fraction rose fairly steadily for the rest of the mission up to quarter 17 when 24% of the cool KOIs were observed in short cadence mode producing a total of 25 million short cadence data.

We obtained the light curve data through the the Barbara A. Mikulski Archive for Space Telescopes[6] (MAST) using Data Release 21 for Quarters 0 through 14, release 20 for Quarter 15, and releases 22 and 23 for Quarters 16 and 17, respectively. For all *Kepler* data header keyword definitions, we refer the reader to the *Kepler* Archive Manual.[7] We consider only those data with SAP QUALITY values equal to 0. This excludes data that were taken under non-optimal circumstances or were flagged for other reasons. On average, this resulted in a rejection of about 12.5% of long cadence data per target and 6.2% of short cadence data per target.

For each KOI, both the Pre-search Data Conditioning (PDCSAP; Smith et al. 2012; Stumpe et al. 2012) and Simple Aperture Photometry (SAP) data were examined. The SAP data were cotrended using the first five cotrending basis vectors available through the MAST website, and then deblended using the FLFRCSAP and CROWDSAP header keywords. In all cases, our calibrated SAP data appeared very similar or nearly identical to the PDSCAP data and as our default we use the PDCSAP data for all KOIs for the sake of uniformity.

Before addressing the transit signals, we first look at the raw data for anomalies, trends, and other potential problems.

[6] https://archive.stsci.edu/kepler

[7] See http://archive.stsci.edu/kepler/manuals/archive_manual.pdf.

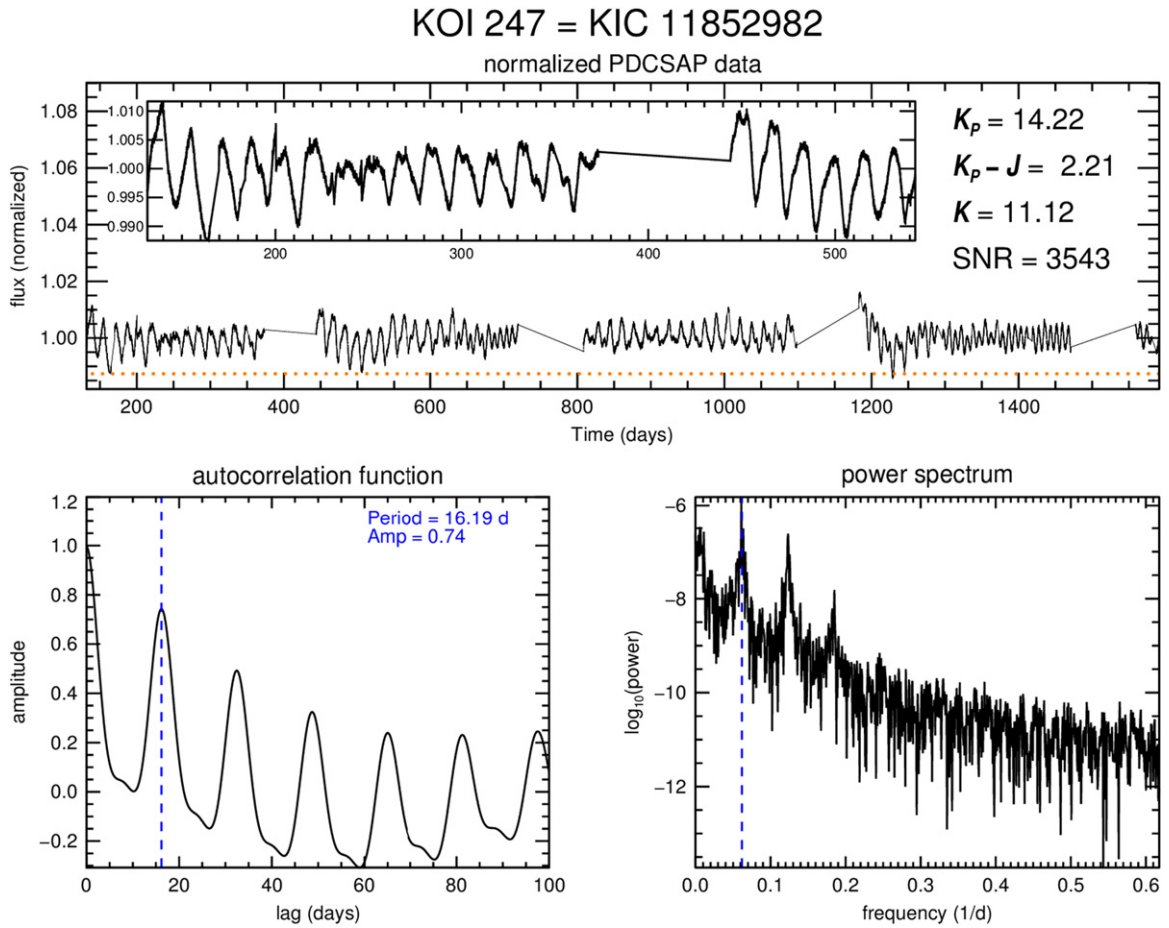

Figure 1. Example of a diagnostic plot for the long cadence data of KOI-247 showing the out of transit data characteristics including the signal to noise of the light curve and absolute photometry. The top panel shows the entire span of the long cadence data set with a zoom in window of the first 400 days. The transit times are marked on the upper panel plot color coded by KOI planet candidate number assignment (.01 = orange; .02 = purple; .03 = gray; .04 = cyan; .05 = magenta). The lower panels show periodicities in the out of transit data via the auto-correlation function (lower left) and Fourier transform (lower right) from which we estimate the stellar rotation period. The vertical lines (dashed blue) denote the peak of the auto-correlation function and its corresponding frequency.

(The complete figure set (104 images) is available.)

Figure 1 shows an example of one of our diagnostic plots that displays the entire time series of data, a zoom in of a small portion of the data, and photometry information. A normalized flux series is created for each KOI in our list by concatenating all of the available data normalized by the median flux value of each quarter. We then subtract the median flux of the combined series and blank out any transit signals using the durations and ephemerides provided by the Exoplanet Archive. These data are then gridded onto a uniform time series and zeroed at values where data were missing. Periods were searched out to 100 days using both an auto-correlation and a Fourier transform. The normalized light curves, auto-correlation functions, and spectral power density were then inspected by eye. In a majority of cases where periodic signatures were seen, they are interpreted as modulations due to the combination of stellar rotation and a non-uniform stellar surface brightness.

3.2. Extracting Transit Signals

Each of the 163 planet signals described above was extracted from the full *Kepler* light curve by fitting a linear drift to the out of transit data extending two transit durations before the beginning of ingress and two durations after egress. For KOIs with multiple candidate planet signals, all other signals were blanked from the time series data before extraction. The transit times and durations used in this process were taken from the Exoplanet Archive. Some sources with large TTVs (such as KOI-314) required a larger buffer. Linear ephemerides were assumed for each of the transit signals in the extraction process. However, a small buffer of 10% of the reported transit duration was used to account for any potential TTVs or errors in the values reported by the Exoplanet Archive. The rms value of the residuals to the linear trend is recorded and applied to all of the data from each transit event as the relative flux error.

Next, each transit signal was confirmed using a box-least-squared algorithm (BLS; Kovács et al. 2002) optimized to oversample the projected BLS peak width by a factor of three (see Ofir 2014). This typically produced convincing transit signals with durations and ephemerides that were generally in agreement with the values of the Exoplanet Archive. However, there were a few exceptions. KOI-1686.01 and KOI-1408.02[8] do not show a convincing transit signal and have been left off our list. Also, the period reported for KOI-1725 was found to

[8] In the latest release from the Exoplanet Archive, these sources are designated as False Positives (Mullally et al. 2015).

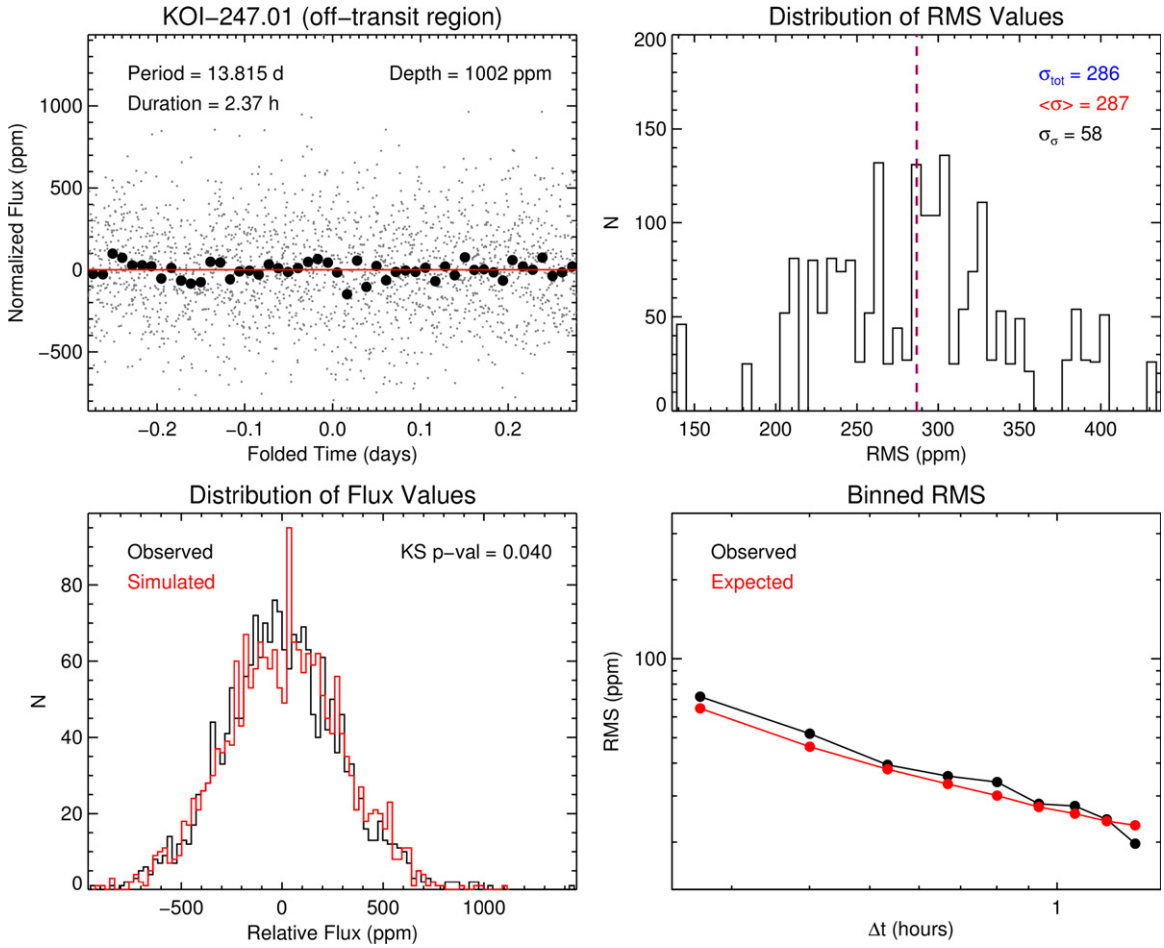

Figure 2. (Top left) The adjacent, transit-free section of the light curve for the specified KOI is shown folded on the period of the planet transit signal. The calibrated *Kepler* data are shown as small dots, and binned data are plotted as larger dots to reveal more subtle structure. (Top right) The distribution of rms values derived from the detrending process are shown in histogram form. The rms of the folded data, $\sigma_{\rm tot}$, is depicted with the blue dotted line; the mean of the rms values derived from the detrending process, $\langle\sigma\rangle$, is shown as the dotted red line; and the spread in the detrend derived rms values, σ_σ, is also displayed. (Bottom left) Histogram of the data from the top left panel is shown and compared with a histogram of values drawn from a normal distribution with zero mean and a standard deviation equal to the rms of the data. The results from a two-sided Kolmogorov–Smirnov test show the probability that the two distributions were drawn from the same parent sample. (Bottom right) The phase folded data are binned on a series of timescales, Δt, starting with the smallest bin which will include at least 20 points and stepping up in 10 bins to one half of the transit duration as reported by the *Kepler* team. This curve is shown in relation to the expected trend (e.g., Winn et al. 2008).

(The complete figure set (163 images) is available.)

be approximately nine minutes off, necessitating an independent period search to adequately retrieve this signal. In cases where a transit signal was apparent in long cadence data, but problematic or not clearly seen in the short cadence data (typically due to a paucity of short cadence data), the transit parameters derived from the long cadence data were applied to the short cadence data. Examples of extracted transit signals are shown in Section 4.

Correlated noise produced by either instrumental or astrophysical phenomena can have a significant affect on the interpretation of astronomical light curve data (see, e.g., Pont et al. 2006; Carter & Winn 2009). Therefore, in addition to the transit extraction, a section of the light curve with no transit signal was extracted in exactly the same manner as the transit signal, but according to a mid-transit time advanced by five times the reported transit duration. This produced a transit-free section of the light curve immediately adjacent to the extracted transit events. Figure 2 shows one example of a "blank" extraction as well as the basic analyses we use to assess the noise properties of our data (see caption for more details). We find that the distribution of data values for each KOI can be reasonably described by a single parameter, σ, and compares well with synthetic, Gaussian distributed data (typical KS p values $\gtrsim$0.01). The fact that the noise properties of our data sample appear to be nearly Gaussian can be attributed to a variety of factors. One dominant effect is that the stars in our sample are by design faint, meaning that the photon noise is higher than for the rest of the sample, which can mask subtler, correlated phenomena. Also, the astrophysical noise from M dwarf light curves is typically caused by inhomogeneities in the stellar surface brightness coupled with stellar rotation rather than pulsation modes (see, e.g., Rodríguez-López et al. 2012). The stellar rotation timescales are typically much longer than the transit durations, and so these effects are adequately corrected with our detrending process. We therefore do not consider the effects of correlated noise in later analyses.

The final step in the preparation of our light curves is outlier rejection. This procedure removes astrophysical (e.g., flares) and instrumental effects not accounted for in the above procedures as well as points that were not adequately

Table 1
Transit Parameters for Long Cadence Fits

KOI	P (days)	δP (s)	t_0 BJD-2454833	δt_0 (s)	$R_p/R_\star$ (%)	$\delta R_p/R_\star$ (%)	$\tau_{\rm tot}$ (hr)	$\delta\tau_{\rm tot}$ (minutes)	b	δb
247.01	13.815050	1.67	858.062061	50.82	2.909	0.225	2.2848	5.400	0.45	0.31
248.01[a]	7.203854	0.51	861.856433	30.55	4.105	0.111	2.5224	2.808	0.36	0.24
248.02[a]	10.912760	1.56	868.268258	57.09	3.338	0.234	2.5104	5.544	0.38	0.28
248.03	2.576571	0.22	860.071548	36.26	2.677	0.217	1.7088	4.176	0.47	0.32
248.04	18.596124	4.60	866.513352	90.03	2.744	0.231	2.3376	6.768	0.47	0.32
249.01	9.549275	0.43	863.305359	17.86	4.046	0.225	1.5960	2.952	0.45	0.30
250.01[a]	12.283005	0.80	845.963352	27.46	5.067	0.213	2.7624	3.888	0.41	0.30
250.02[a]	17.251179	1.74	857.185157	43.44	4.367	0.266	1.9608	5.184	0.51	0.29
250.03	3.543902	0.79	859.215985	95.76	1.838	0.154	2.1216	7.272	0.43	0.30
250.04	46.827733	8.12	885.988374	75.71	3.907	0.227	1.8696	5.688	0.46	0.30
251.01	4.164384	0.15	858.211584	14.39	4.678	0.194	1.8192	2.664	0.42	0.27
251.02	5.774417	2.35	860.544378	153.87	1.549	0.109	1.8288	8.064	0.48	0.33
252.01	17.604618	2.09	857.078072	49.29	4.641	0.340	3.6984	8.208	0.58	0.27
253.01	6.383165	0.53	859.985599	33.82	4.271	0.287	1.8120	4.032	0.43	0.29
253.02	20.618078	12.75	867.149460	318.82	2.382	0.212	3.2160	15.912	0.48	0.33
254.01	2.455241	0.01	863.199607	1.40	19.063	0.818	1.8336	1.152	0.56	0.04
255.01	27.522008	2.78	850.351246	43.24	4.583	0.199	4.1208	4.680	0.37	0.25
255.02	13.602938	12.77	861.366322	369.59	1.375	0.127	2.8056	15.264	0.48	0.33
314.01[a]	13.781096	0.77	853.126068	22.01	2.514	0.117	2.3016	3.024	0.49	0.31
314.02[a]	23.088964	2.42	863.679273	44.00	2.277	0.113	1.7736	3.456	0.46	0.30
314.03[a]	10.313231	4.37	855.441694	149.86	1.084	0.066	1.9992	6.336	0.48	0.33
463.01[a]	18.477644	1.32	868.940991	29.86	4.923	0.160	1.8288	2.808	0.35	0.24
478.01	11.023478	0.68	854.569829	22.75	4.033	0.192	1.3968	3.024	0.40	0.29
531.01	3.687470	0.03	860.437248	3.85	5.677	0.601	1.0272	1.512	0.31	0.20
571.01	7.267302	0.89	857.440913	49.58	2.506	0.133	2.2872	4.680	0.43	0.32
571.02	13.343016	2.20	857.396606	63.93	2.737	0.171	2.7600	5.328	0.47	0.32
571.03	3.886785	0.46	860.160360	49.69	2.125	0.147	1.9008	4.824	0.47	0.32
571.04	22.407609	6.06	870.846301	110.16	2.468	0.135	3.3288	7.920	0.47	0.31
571.05	129.943525	147.13	826.551452	441.38	2.111	0.168	5.8080	23.400	0.49	0.34
596.01	1.682696	0.10	860.358616	24.01	2.501	0.123	1.4184	2.664	0.41	0.28
641.01	14.851847	1.58	861.184378	47.21	3.263	0.153	3.3552	4.752	0.39	0.27
739.01	1.287077	0.10	862.263195	31.16	2.679	0.107	1.4568	3.024	0.44	0.32
781.01	11.598224	1.21	853.092509	43.37	5.152	0.319	2.5224	4.968	0.43	0.28
812.01	3.340220	0.28	860.063988	34.38	4.009	0.169	1.9224	3.312	0.41	0.28
812.02	20.060375	5.21	869.639153	107.38	3.806	0.220	3.3552	7.488	0.41	0.28
812.03	46.184176	22.54	904.183430	193.55	3.744	0.207	4.7712	12.312	0.45	0.32
812.04	7.825033	3.73	856.457413	194.71	2.321	0.198	2.2248	11.232	0.47	0.33
817.01	23.967927	6.72	857.325190	131.08	3.411	0.183	3.8664	9.720	0.49	0.31
817.02	8.295585	1.47	840.919728	74.93	2.868	0.252	1.1616	6.120	0.46	0.32
818.01	8.114381	0.89	857.947143	47.90	3.899	0.212	2.2608	4.608	0.45	0.29
854.01	56.056171	21.46	817.783856	162.12	3.946	0.221	4.5552	12.456	0.50	0.31
886.01[a]	8.010828	2.07	859.135626	116.70	3.586	0.318	2.5080	9.216	0.56	0.30
886.02[a]	12.071357	6.10	867.740134	237.23	2.433	0.173	4.5336	10.584	0.31	0.23
886.03	20.995946	10.18	845.184612	215.08	2.553	0.183	2.9544	12.168	0.48	0.33
898.01[a]	9.770453	1.29	849.875896	55.18	4.370	0.165	2.4216	4.248	0.41	0.28
898.02	5.169805	0.85	865.384993	67.98	3.207	0.218	2.2200	6.912	0.51	0.32
898.03	20.090234	5.88	871.224471	120.16	3.701	0.263	3.6840	10.512	0.50	0.32
899.01	7.113716	0.99	864.355699	58.81	2.701	0.164	2.1624	5.184	0.47	0.30
899.02	3.306546	0.52	861.814312	60.46	2.163	0.163	1.8168	5.832	0.46	0.32
899.03	15.368446	3.41	854.339483	95.93	2.652	0.173	2.4936	7.200	0.47	0.32
936.01	9.467811	0.52	869.566887	23.44	4.459	0.146	2.4552	2.808	0.35	0.24
936.02	0.893042	0.04	861.475877	17.66	2.645	0.132	1.0968	2.376	0.43	0.29
947.01	28.599142	4.45	847.706511	66.99	3.859	0.141	3.6744	5.400	0.38	0.27
952.01	5.901277	0.65	861.858407	48.55	3.943	0.153	2.2272	4.320	0.43	0.29
952.02[a]	8.752103	1.67	862.049430	82.39	3.819	0.316	2.3328	8.208	0.55	0.30
952.03	22.780766	4.08	861.404117	77.15	4.455	0.118	3.1992	4.824	0.38	0.27
952.04	2.896015	0.94	860.512106	153.00	1.957	0.194	2.0496	10.944	0.43	0.30
952.05	0.742962	0.23	860.636153	122.51	1.400	0.122	1.2984	6.768	0.46	0.32
961.01	1.213770	0.03	862.333219	9.88	4.211	0.268	0.5448	1.512	0.45	0.30
961.02	0.453288	0.00	861.396478	3.98	3.854	0.130	0.5040	0.792	0.35	0.24
961.03	1.865114	0.08	861.186344	18.22	3.615	0.274	0.4512	2.088	0.44	0.31
1078.01	3.353728	0.35	862.627731	44.73	3.536	0.256	1.5672	5.040	0.47	0.33
1078.02	6.877453	0.76	861.094063	48.02	3.977	0.220	1.3248	4.104	0.44	0.31

Table 1
(Continued)

KOI	P (days)	δP (s)	t_0 BJD-2454833	δt_0 (s)	$R_p/R_\star$ (%)	$\delta R_p/R_\star$ (%)	$\tau_{\rm tot}$ (hr)	$\delta\tau_{\rm tot}$ (minutes)	b	δb
1078.03	28.464536	7.56	869.653492	114.85	4.035	0.200	2.8272	7.848	0.43	0.30
1085.01	7.717951	3.44	864.639733	218.11	1.679	0.153	2.2776	11.880	0.46	0.32
1141.01	5.728131	1.70	862.652205	115.59	2.534	0.156	2.0208	7.128	0.47	0.32
1146.01	7.097120	2.63	860.244823	161.55	1.897	0.136	2.2536	9.792	0.47	0.33
1201.01	2.757592	0.43	861.053399	80.52	2.227	0.139	1.3032	4.248	0.46	0.32
1393.01	1.694740	0.11	972.242566	24.30	3.679	0.170	1.6800	3.312	0.45	0.30
1397.01	6.247032	0.74	969.118946	42.16	3.878	0.182	1.4376	3.816	0.44	0.31
1408.01	14.534055	4.46	857.599004	121.33	2.163	0.132	3.3336	7.632	0.46	0.30
1422.01	5.841635	0.84	866.127692	59.12	3.587	0.261	1.9464	5.328	0.44	0.30
1422.02	19.850252	5.28	848.261297	112.57	3.837	0.312	2.8968	8.424	0.45	0.30
1422.03	10.864435	4.70	869.906646	185.64	2.624	0.318	2.1936	14.400	0.48	0.34
1422.04	63.336340	53.61	795.964581	297.62	3.164	0.252	3.4944	15.408	0.46	0.32
1422.05	34.141951	24.69	853.022724	340.15	2.658	0.306	3.2760	21.528	0.47	0.33
1427.01	2.613018	0.50	862.145224	76.69	2.405	0.150	1.8456	5.760	0.47	0.32
1649.01	4.043551	1.15	859.463541	106.02	1.831	0.177	1.4856	7.632	0.44	0.32
1681.01	6.939112	2.21	860.005991	121.03	2.397	0.226	2.2488	10.296	0.45	0.31
1681.02	1.992809	0.66	861.073462	146.79	1.568	0.162	1.6440	9.864	0.44	0.31
1681.03	3.531068	1.32	861.721450	160.98	1.706	0.192	1.5096	10.368	0.46	0.33
1702.01	1.538181	0.13	880.916015	33.51	2.766	0.237	1.0800	4.104	0.43	0.30
1725.01	9.878652	0.89	859.552053	43.38	3.711	0.182	1.9248	3.096	0.42	0.29
1843.01	4.194497	0.40	847.198436	43.57	2.515	0.202	1.7760	5.904	0.52	0.33
1843.02	6.355838	2.74	843.001063	189.46	1.220	0.123	1.4904	9.576	0.48	0.33
1867.01	2.549564	0.30	861.781789	48.16	2.216	0.101	1.6512	3.816	0.45	0.32
1867.02	13.969499	1.68	844.614392	50.81	3.178	0.194	1.3584	4.392	0.45	0.30
1867.03	5.212318	1.20	857.220810	86.34	2.007	0.154	2.1672	6.192	0.48	0.32
1868.01	17.760788	2.29	865.699188	52.22	3.525	0.197	1.6248	4.536	0.45	0.32
1879.01	22.085589	3.93	974.483549	56.76	5.267	0.371	2.2080	5.976	0.47	0.30
1880.01	1.151167	0.05	861.920492	16.61	2.355	0.083	1.0488	1.944	0.50	0.33
1902.01	137.864485	24.66	862.133272	74.31	4.050	0.719	1.7112	9.432	0.44	0.34
1907.01	11.350118	1.81	860.450521	69.52	3.333	0.206	2.2992	5.976	0.46	0.31
2006.01	3.273459	0.43	861.155294	54.02	1.543	0.070	1.6920	3.672	0.49	0.32
2036.01	8.410996	2.19	857.144315	106.06	2.616	0.236	2.3592	8.136	0.43	0.30
2036.02	5.795327	3.26	855.404252	196.06	1.787	0.178	2.3040	11.664	0.47	0.33
2057.01	5.945659	1.28	865.310547	88.88	1.952	0.184	2.2392	7.344	0.41	0.29
2058.01	1.523729	0.23	861.485510	60.77	1.769	0.165	1.3776	6.480	0.43	0.30
2090.01	5.132484	0.79	973.887826	52.79	2.847	0.161	1.4952	4.464	0.45	0.30
2130.01	16.855930	5.54	863.073317	168.40	3.012	0.229	2.4792	13.608	0.50	0.34
2156.01	2.852353	0.25	859.393812	36.64	3.640	0.281	0.7728	3.384	0.44	0.31
2179.01	14.871553	4.24	970.498340	105.09	2.969	0.170	2.4864	6.840	0.46	0.31
2179.02	2.732765	0.43	971.700991	54.36	2.445	0.151	1.0488	3.816	0.46	0.32
2191.01	8.847876	2.52	847.979545	125.58	1.987	0.184	2.2728	9.648	0.38	0.28
2238.01	1.646802	0.22	861.594051	54.26	1.603	0.137	1.2600	5.472	0.42	0.30
2306.01	0.512407	0.04	860.882688	32.66	1.729	0.119	1.0944	2.952	0.45	0.30
2329.01	1.615360	0.21	861.312567	53.06	2.159	0.237	1.0896	6.120	0.43	0.32
2347.01	0.588001	0.05	861.179765	33.63	1.657	0.105	1.1352	3.312	0.46	0.32
2417.01	47.705251	42.29	1052.717647	307.98	3.393	0.352	5.6904	21.744	0.50	0.33
2418.01	86.829090	113.66	883.909263	507.11	2.674	0.281	6.1656	32.760	0.49	0.34
2453.01	1.530516	0.15	860.392109	40.99	2.564	0.244	0.5664	3.672	0.48	0.34
2480.01	0.666826	0.06	861.216259	39.08	2.247	0.186	0.7680	3.744	0.46	0.32
2542.01	0.727330	0.11	844.428343	69.24	1.810	0.139	0.9360	4.608	0.46	0.32
2626.01	38.097253	23.14	863.851953	268.07	2.965	0.263	3.3552	16.560	0.46	0.32
2650.01	34.989404	29.93	879.002425	358.94	2.306	0.186	4.4328	16.848	0.45	0.32
2650.02	7.054276	3.27	862.780386	217.51	1.848	0.196	1.7640	11.592	0.46	0.33
2662.01	2.104337	0.36	861.414256	71.87	1.504	0.103	1.0320	4.536	0.47	0.33
2704.01	4.871225	0.68	1068.916908	42.36	10.241	0.521	1.5552	4.464	0.33	0.24
2704.02	2.984151	0.69	1064.175129	64.21	6.679	0.352	1.3272	4.536	0.40	0.28
2704.03	8.152687	9.42	1063.603281	305.72	5.227	0.823	2.3928	28.800	0.48	0.36
2705.01	2.886761	0.26	1064.090471	29.89	2.350	0.233	0.9024	3.672	0.42	0.30
2715.01	11.128299	1.85	1052.062093	54.55	8.127	0.579	2.6784	8.280	0.56	0.27
2715.02	2.226489	0.52	1066.274948	75.48	4.334	0.366	1.8312	6.696	0.43	0.30
2715.03	5.720880	2.22	1067.165009	135.79	4.017	0.204	2.4888	7.848	0.44	0.31
2764.01	2.252974	0.58	970.347138	91.65	2.146	0.176	1.7280	7.056	0.47	0.33
2793.01	4.496868	0.91	1159.490499	53.06	4.541	0.262	1.7712	4.464	0.43	0.30

Table 1
(Continued)

KOI	P (days)	δP (s)	t_0 BJD-2454833	δt_0 (s)	$R_p/R_\star$ (%)	$\delta R_p/R_\star$ (%)	$\tau_{\rm tot}$ (hr)	$\delta\tau_{\rm tot}$ (minutes)	b	δb
2793.02	1.766790	0.52	1163.121258	80.97	3.134	0.213	1.4088	5.112	0.47	0.33
2839.01	2.164573	0.59	954.368569	98.60	2.202	0.161	1.3512	6.480	0.48	0.33
2842.01	1.565414	0.15	1111.295284	29.66	5.349	0.465	0.8136	3.600	0.45	0.32
2842.02	5.148931	1.10	1111.615116	67.33	4.999	0.428	0.9672	5.400	0.47	0.33
2842.03	3.036220	0.60	1108.684748	60.98	4.362	0.477	0.9840	5.184	0.46	0.33
2845.01	1.574091	0.40	860.664033	111.13	1.519	0.114	1.5720	6.624	0.48	0.33
2862.01	24.575351	12.26	979.739313	179.76	2.938	0.253	2.2104	11.160	0.45	0.32
2926.01	12.285498	7.52	1151.595094	162.99	4.138	0.221	3.0240	9.144	0.45	0.32
2926.02	5.536076	2.53	1161.594913	125.53	3.513	0.197	2.0880	7.992	0.46	0.32
2926.03	20.956929	14.59	1165.968351	195.86	4.371	0.281	3.6384	12.600	0.47	0.32
2926.04	37.634156	64.86	1212.535073	386.23	3.936	0.241	4.4088	17.064	0.45	0.30
2992.01	82.659402	73.12	813.954445	283.72	3.618	0.538	3.8616	22.824	0.50	0.36
3010.01	60.866573	61.58	909.679601	375.88	2.850	0.236	4.7664	22.824	0.49	0.33
3034.01	31.020889	18.05	851.497786	195.00	2.836	0.260	1.8744	11.664	0.45	0.33
3094.01	4.577003	0.93	859.843063	89.46	2.494	0.249	0.9528	5.832	0.48	0.33
3102.01	9.326378	7.39	855.995807	315.73	1.735	0.191	2.0472	14.688	0.47	0.33
3119.01	2.184432	0.59	1066.429336	82.53	4.129	0.357	1.1352	5.904	0.45	0.32
3140.01	5.688796	3.74	859.832880	254.73	1.478	0.134	2.7576	13.536	0.45	0.32
3144.01	8.073945	4.10	1048.697851	186.12	3.132	0.220	2.1888	9.792	0.45	0.32
3263.01	76.879365	4.69	761.917120	22.49	14.917	3.046	2.3928	5.760	0.68	0.29
3282.01	49.276798	31.03	846.901733	269.07	3.575	0.292	3.7872	18.000	0.48	0.33
3284.01	35.233209	22.62	840.028855	328.10	1.879	0.194	3.8328	20.160	0.43	0.31
3414.01	27.009809	0.29	897.564195	3.69	33.676	4.891	2.0016	2.520	0.79	0.09
3444.01	12.671432	7.50	859.778161	244.73	1.254	0.115	2.4624	12.456	0.45	0.32
3444.02	60.326669	4.09	868.978630	30.12	4.568	0.524	1.5168	4.104	0.33	0.25
3444.03	2.635964	1.19	859.838096	195.82	0.872	0.088	1.5816	10.008	0.46	0.32
3444.04	14.150370	8.32	848.976183	260.63	1.212	0.139	1.6656	12.888	0.47	0.33
3497.01	20.359756	5.95	846.882413	137.23	1.677	0.146	1.9320	9.432	0.47	0.33
3749.01	10.727244	3.98	851.628048	12.96	33.302	7.451	1.8216	4.176	0.86	0.13
4087.01	101.111336	74.93	923.296793	294.74	2.948	0.136	8.0304	16.560	0.45	0.31
4252.01	15.571357	7.85	852.870658	213.79	1.199	0.122	2.1600	12.672	0.43	0.31
4290.01	4.838142	5.92	725.405466	114.25	4.610	0.360	1.2768	7.128	0.45	0.31
4427.01	147.661348	110.51	982.258277	382.50	3.205	0.257	6.1056	20.160	0.44	0.30
4875.01	0.912184	0.49	861.553074	207.01	1.211	0.142	1.1280	11.232	0.47	0.33
5228.01	546.280708	5544.62	880.611075	4355.96	2.483	0.413	33.9576	302.760	0.52	0.36
5359.01	2.719979	15.24	584.861009	257.65	2.783	0.255	2.0352	12.312	0.46	0.33
5692.01	2.641814	1.62	861.675662	244.83	0.754	0.071	2.3232	13.752	0.45	0.32

Note.
[a] Transit parameters derived from fits to individual transit times. Period and mid-transit time are used from fits assuming linear ephemeris.

detrended. We reject outliers from the phase folded transit signal by binning the data into bins that are one half the integration time of the observations or with widths that contain at least 20 data points per bin. From the distribution of data points in each bin, a robust estimation of the standard deviation is calculated using the median absolute deviation:

$$\mathrm{MAD} = \mathrm{median}\Big(\big|x_i - \mathrm{median}(\boldsymbol{x})\big|\Big), \quad (1)$$

where the residuals are given by $\boldsymbol{x} = \{x_0, x_1 \ldots x_n\}$. MAD is then scaled to estimate the standard deviation assuming a Gaussian distribution so that $\sigma = 1.4826\,\mathrm{MAD}$, and then data are rejected with absolute deviation from the median beyond a threshold $n\sigma$, where

$$n = \sqrt{2}\ \ \mathrm{erf}^{-1}(1 - \eta/N), \quad (2)$$

and where N is the number of data point under consideration. Removing outliers in this manner produces a minimal effect on the statistical properties of the data by removing points that are inconsistent with the original robust estimation of the standard deviation of the sample given the sample size. We use a value of $\eta = 0.1$ which translates to $2.8 \lesssim n \lesssim 4.0$ for our data set.

4. TRANSIT FITTING

4.1. Long and Short Cadence Fits Using a Linear Ephemeris Model

We characterize our vetted sample of 163 planet candidates around 104 cool stars by first fitting all of the long and short cadence data available with a linear ephemeris transit model using a Markov Chain Monte Carlo parameter estimation algorithm. Our light curve model uses the analytic solutions from Mandel & Agol (2002) for a quadratic stellar limb darkening law that provides a relative flux model for planet-to-star size ratio, projected separation, and limb darkening parameters. The hyper-geometric functions of those solutions need to be evaluated numerically and present a computational barrier. We therefore use a circular planet orbit to convert time

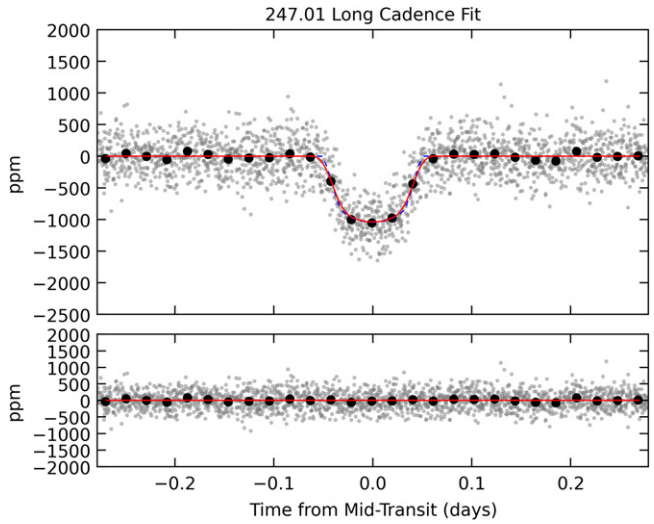

Figure 3. Phase folded long cadence data for KOI-247.01 are shown as gray dots. These data binned at a timescale approximately equal to the original sampling of the long cadence data stream are shown as black dots for viewing purposes only. The best-fit model is shown in red and the residuals of this fit are shown in the bottom panel. The raw model (without resampling) is shown as a blue dashed line for reference.

(The complete figure set (163 images) is available.)

into projected separation for a given period and transit duration. This allows us to side-step solving *Kepler*'s equation, and instead perform the transformation from time to relative separation between the star and planet with simple trigonometric functions. Under this approximation, the ingress and egress of the model are exactly symmetric, also halving the number of computations needed for each model call. Of course, this does not allow for subtle effects due to eccentric orbits to be adequately modeled and care must be taken when interpreting the derived transit duration in terms of stellar density (Seager & Mallén-Ornelas 2003; Kipping 2010b). However, for our sample, this effect can be accounted for and is expected to have a negligible effect on the derived transit parameters.

We parametrize our model with the scaled planet radius, $R_p/R_\star$; the impact parameter, b; the duration from the first to the fourth contact point of the transit, $\tau_{\rm tot}$; the time of mid-transit as measured nearest to the middle of the *Kepler* light curve, t_0; the period, P; and two limb darkening parameters, q_1 and q_2, which characterize the full range of quadratic parameter space of monotonically decreasing and positive value profiles (Kipping 2013).

Before our models can be compared to data, the effect of finite integration times must be considered (e.g., Kipping 2010a; Price & Rogers 2014). The *Kepler* Mission produced time series data sampled at two different intervals using a single exposure time. The exposure time (accumulated time of flux from a celestial source on a given pixel) is $t_{\rm exp} = 6.020$ s, and for every exposure there is a fixed CCD readout time of $t_{\rm read} = 0.519$ s. The short cadence data is made up of nine such exposures and therefore the time between the start of successive short cadence data is $(t_{\rm exp} + t_{\rm read}) \times 9 = 58.849$ s. However, the time interval over which the astronomical signal is integrated is one read shorter than this, i.e., $t^{\rm short}_{\rm smooth} = 9t_{\rm exp} + 8t_{\rm read} = 58.330$ s. Similarly, the long cadence data are made up of 270 integrations and therefore the time between successive integration times is $t^{\rm long}_{\rm cadence} = 1765.463$ s and the smoothing time $t^{\rm long}_{\rm smooth} = 1764.944$ s.

To account for the effects of integration time, we first calculate the planet path across the stellar disk assuming that the planet is in a circular orbit using $b = a\cos(i)/R_\star$. The light curve for this planetary trajectory is oversampled and then smoothed using a uniform filter of width $t_{\rm smooth}$. This is analogous to the resampling procedure recommended by Kipping (2010a), and we hereafter refer to this process as resampling. The degree of resampling needed to produce an accurate model using this method will depend on the transit parameters. Therefore, we numerically determine the optimal resampling for each transit candidate based on the parameters from preliminary fits enforcing an resampling of at least five. For a grid of transit parameter values spanning the full range of $R_p/R_\star$ and $\tau_{\rm tot}$ in our data set, and for an impact parameter of 0 (the effect of finite integration time is most severe for low impact parameter transits), we first calculate a reference transit model resampled by a factor of 3001. We then calculate transit curves for the same set of input parameters resampled in steps of 2 from 3 to 501. The smallest resampling value that produces peak-to-peak discrepancies with the reference model of less than one part per million is then recorded. We then construct a grid of values from this procedure that we use to interpolate the optimal resampling values to be used for any of our targets based on their preliminary transit parameters.

We use a Bayesian framework to determine the best fit values for our seven model parameters and their associated errors. To evaluate the likelihood, we do not resample the model at each data timestamp. Instead, we phase fold the data at each trial period, P, and mid-transit time, t_0, and interpolate our resampled model to the phase folded timestamps of the data. This speeds up each likelihood call by an order of magnitude or more. The quantity $(R_p/R_\star)^2$ is a scale parameter in the problem and we therefore apply a Jefferys prior to this parameter. We note that this has a small to negligible effect on our posterior samples as we are data-dominated rather than prior-dominated for the majority of our transit candidates. Each of the other free parameters have uniform priors (i.e., no prior).

We use the `emcee` affine invariant Markov Chain Monte Carlo ensemble sampler (Foreman-Mackey et al. 2013) with 1000 chains, or "walkers" ($n_w = 1000$). The initial values of each walker were over-dispersed in most parameters based on the estimated values found by fitting the transit shape with a quick and flexible Levenberg–Marquardt fitting algorithm (Markwardt 2009). The relative planet radius, $R_p/R_\star$, is dispersed in a uniform manner from 0 to a factor of 2 larger than the value obtained from the preliminary fit; the full duration, $\tau_{\rm tot}$, is dispersed from half to twice the preliminary fit value; the impact parameter, b, is dispersed uniformly from 0 to 1; the period, P, is dispersed by ± 1 s from the nominal value; the mid-transit times, t_0, uniformly span 2 minutes; and the limb darkening parameters, q_1 and q_2, are uniformly dispersed between 0 and 1.

The walkers are evolved for $n_b = 1000$ steps and then analyzed. We use the correlation length, c_l, to assess if the chains have reached a sufficiently mixed state. The burn-in stage was re-run with a larger number of steps if the number of independent draws, $n_b n_w/c_l$, was found to be less than 10,000. The sampler was then reset and the walkers restarted from their last location for an additional 1000 steps. These last 1000 steps

Table 2
Transit Parameters for Short Cadence Fits

KOI	P (days)	δP (s)	t_0 BJD-2454833	δt_0 (s)	$R_p/R_\star$ %	$\delta R_p/R_\star$ %	$\tau_{\rm tot}$ (hr)	$\delta\tau_{\rm tot}$ (minutes)	b	δb
247.01	13.815048	2.79	816.617079	35.00	2.932	0.094	2.0760	2.016	0.36	0.24
248.01[a]	7.203856	0.68	1063.565400	27.16	4.511	0.128	2.7024	2.448	0.82	0.03
248.02[a]	10.912775	2.26	1064.699387	66.43	3.142	0.099	2.8056	2.016	0.24	0.18
248.03	2.576568	0.18	1063.620781	23.68	2.711	0.135	1.6512	1.800	0.48	0.26
248.04	18.596035	5.66	1071.069820	98.67	2.631	0.217	2.3592	5.904	0.47	0.31
249.01	9.549278	0.75	853.755275	13.74	3.949	0.106	1.5936	1.080	0.29	0.20
250.01[a]	12.282930	1.08	1067.057517	25.08	5.526	0.207	2.9400	2.664	0.81	0.05
250.02[a]	17.251180	2.64	1046.949926	45.84	4.825	0.438	2.1336	4.824	0.76	0.12
250.03	3.543901	0.81	1064.763415	73.09	1.960	0.187	2.0280	4.680	0.52	0.32
250.04	46.827619	11.22	1073.299935	90.27	3.905	0.493	2.0064	7.272	0.72	0.26
251.01	4.164381	0.15	1049.773828	9.61	4.658	0.145	1.7976	1.080	0.37	0.20
251.02	5.774490	4.41	1045.321872	139.32	1.549	0.116	1.7184	7.992	0.48	0.33
252.01	17.604678	2.32	1033.124115	35.64	4.429	0.160	3.5328	2.808	0.35	0.24
253.01	6.383154	0.54	1057.864519	24.52	4.446	0.257	1.7712	2.304	0.61	0.22
253.02	20.617213	26.45	1073.333911	423.48	2.210	0.227	3.8496	21.384	0.46	0.33
254.01	2.455241	0.01	1064.529313	1.62	19.021	0.384	1.8192	0.504	0.53	0.01
255.01	27.521998	3.59	1043.004555	38.58	4.561	0.188	4.1160	3.096	0.39	0.24
255.02	13.603507	22.57	1051.814672	442.25	1.275	0.110	3.1488	14.976	0.48	0.33
314.01[a]	13.781059	0.71	1059.843180	14.34	2.603	0.101	2.3064	1.440	0.63	0.13
314.02[a]	23.089024	2.74	1048.389953	41.93	2.413	0.394	1.9296	5.616	0.68	0.31
314.03[a]	10.313760	5.69	1072.004278	182.45	1.026	0.098	1.8240	8.064	0.39	0.28
463.01[a]	18.477200	12.32	1367.835784	40.59	5.046	0.198	1.8216	2.520	0.35	0.24
531.01	3.687460	0.54	904.686698	7.11	6.278	1.089	1.0848	1.944	0.56	0.27
571.01	7.267344	1.12	1104.529642	45.95	2.533	0.125	2.2560	2.736	0.49	0.29
571.02	13.342947	2.38	1110.913718	48.25	2.727	0.076	2.7720	3.024	0.66	0.23
571.03	3.886790	0.38	1108.913123	31.08	2.107	0.087	1.8504	1.728	0.45	0.28
571.04	22.407795	5.32	1117.331057	88.11	2.423	0.110	3.2640	4.032	0.40	0.28
571.05	129.944005	339.37	1086.446411	900.93	2.147	0.181	5.2536	28.872	0.47	0.32
596.01	1.682697	0.26	865.405753	24.09	2.598	0.140	1.4112	1.944	0.57	0.25
739.01	1.287078	0.26	903.448937	30.66	2.578	0.147	1.5144	2.304	0.51	0.30
812.01	3.340224	0.47	1200.766635	32.11	3.942	0.143	1.9080	2.304	0.39	0.27
812.02	20.060078	15.04	1190.605490	176.60	3.692	0.319	3.5040	10.008	0.45	0.32
812.03	46.184101	46.30	1181.286403	222.49	3.609	0.215	4.9728	12.384	0.44	0.30
812.04	7.825101	6.01	1185.104652	183.34	2.157	0.174	2.3784	8.712	0.46	0.32
817.01	23.967393	39.23	1288.749229	281.41	3.353	0.438	4.0176	17.496	0.55	0.34
817.02	8.295646	5.09	1288.883486	103.50	2.730	0.200	1.1976	5.184	0.46	0.32
854.01	56.053787	99.52	1266.237042	280.44	4.142	0.246	4.7304	11.952	0.48	0.30
886.01[a]	8.009985	9.59	1347.809468	135.95	3.812	0.203	2.4336	7.200	0.84	0.14
886.02[a]	12.072588	31.23	1350.556846	284.08	3.184	0.172	3.0240	5.040	0.39	0.27
886.03	20.995881	56.93	1328.082217	345.37	2.717	0.215	3.0432	16.632	0.50	0.33
898.01[a]	9.770428	1.74	1113.680872	43.37	4.344	0.115	2.4552	2.088	0.40	0.25
898.02	5.169829	0.94	1113.536547	59.64	3.078	0.138	2.2584	2.736	0.37	0.26
898.03	20.090228	10.10	1112.306231	132.13	3.549	0.275	3.8400	9.000	0.57	0.31
899.01	7.113708	1.56	1184.472277	53.03	2.686	0.155	2.1840	3.168	0.50	0.28
899.02	3.306547	0.65	1182.547053	40.07	2.159	0.109	1.7544	2.304	0.47	0.34
899.03	15.368448	5.23	1177.078002	78.63	2.687	0.148	2.4432	4.176	0.46	0.30
936.01	9.467874	3.26	954.776076	27.44	4.564	0.110	2.4624	1.728	0.26	0.18
936.02	0.893039	0.17	953.458458	18.75	2.588	0.109	1.1256	1.152	0.50	0.27
947.01	28.598917	18.95	1276.691772	85.81	3.881	0.175	3.7704	6.552	0.51	0.26
952.01	5.901300	1.55	1162.819235	65.71	4.135	0.507	2.4096	6.480	0.71	0.26
952.02[a]	8.751986	3.96	1168.372434	111.13	3.927	0.240	2.5008	8.136	0.85	0.14
952.03	22.780779	7.94	1180.338720	75.57	4.436	0.134	3.3168	5.760	0.48	0.28
952.04	2.896003	1.47	1164.593353	106.21	2.008	0.165	1.7448	5.400	0.46	0.32
952.05	0.742960	0.25	1163.018720	83.96	1.551	0.117	1.1520	3.960	0.51	0.33
961.01	1.213771	0.02	1199.760924	4.12	4.229	0.116	0.5424	0.360	0.41	0.21
961.02	0.453287	0.01	1199.548330	2.97	4.133	0.128	0.4488	0.288	0.46	0.20
961.03	1.865111	0.05	1200.637140	6.53	3.613	0.123	0.4512	0.504	0.44	0.28
1078.01	3.353711	0.56	1201.355442	47.99	3.615	0.186	1.5840	3.240	0.47	0.33
1078.02	6.877478	1.41	1198.090516	62.73	4.031	0.215	1.2576	2.808	0.43	0.29
1078.03	28.464390	18.41	1182.769700	179.24	3.765	0.227	2.6784	7.848	0.43	0.31
1201.01	2.757584	4.90	954.809350	129.03	2.298	0.277	1.0368	6.912	0.48	0.34
1408.01	14.534993	29.40	1337.221964	439.96	2.046	0.198	2.8776	19.296	0.47	0.33
1725.01	9.878617	1.63	1412.757288	13.37	3.698	0.126	1.9248	1.368	0.39	0.21

Table 2
(Continued)

KOI	P (days)	δP (s)	t_0 BJD-2454833	δt_0 (s)	$R_p/R_\star$ %	$\delta R_p/R_\star$ %	$\tau_{\rm tot}$ (hr)	$\delta\tau_{\rm tot}$ (minutes)	b	δb
1843.01	4.194588	1.98	1329.565344	55.83	2.409	0.206	1.8768	3.960	0.47	0.32
1843.02[b]	6.355921	33.60	1332.399317	1539.87	0.002	0.008	6.1416	574.128	0.50	0.34
1867.01	2.549561	1.57	1346.199599	62.28	2.282	0.236	1.7880	5.040	0.74	0.28
1867.02	13.969476	8.67	1333.548100	76.73	3.196	0.335	1.3968	4.824	0.49	0.33
1867.03	5.212287	3.18	1347.174910	78.00	2.139	0.099	2.1480	3.960	0.46	0.33
2036.01	8.410908	45.64	1521.619841	258.10	2.885	0.286	2.1720	11.376	0.47	0.32
2036.02[b]	5.795352	33.41	1516.076576	3536.86	0.000	0.001	20.6520	1105.416	0.50	0.34
2418.01	86.806562	496.84	1404.881538	1138.05	2.811	0.382	6.7512	57.816	0.49	0.34
2650.01	34.987138	95.73	1368.842232	475.54	2.088	0.895	4.2984	20.088	0.48	0.33
2650.02	7.054275	22.60	1342.482081	404.28	1.777	0.244	1.7520	16.272	0.48	0.33
2704.01	4.869934	121.13	1575.526914	225.74	22.127	2.903	2.0088	15.840	0.49	0.33
2704.02	2.983711	161.90	1574.470943	525.50	14.312	17.881	1.7064	39.456	0.56	0.36
2704.03[b]	8.176432	4321.04	1569.090938	1618.76	0.000	0.000	45.5976	1875.672	0.50	0.33
2842.01	1.565443	7.63	1574.656534	57.51	5.535	0.415	0.7728	2.736	0.44	0.30
2842.02	5.149013	28.07	1575.020298	120.44	5.349	0.601	0.8496	5.544	0.45	0.32
2842.03	3.036239	16.96	1576.259874	232.30	4.132	2.533	1.0056	12.456	0.47	0.33

Notes.
[a] Transit parameters derived from fits to individual transit times. Period and mid-transit time are used from fits assuming linear ephemeris.
[b] Transit fit failed due to insufficient data.

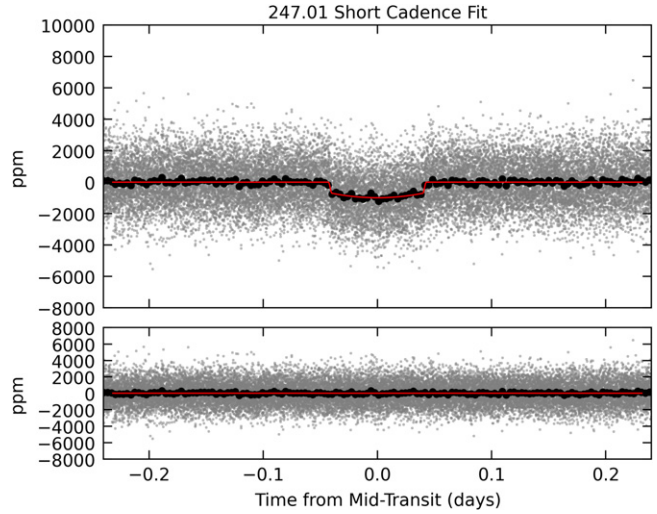

Figure 4. Same as Figure 3, but for the KOI-247.01 short cadence data.
(The complete figure set (79 images) is available.)

for each 1000 walkers (10^6 samples total) comprise the final posterior samples that we use to estimate the transit parameters.

The results of the long cadence data fits are summarized in Table 1, and an example fit can be seen in Figure 3. A fit to the short cadence data for this same KOI can be seen in Figure 4. The median values for planet period, mid-transit time, relative radius, duration, and impact parameter are reported along with the half width of the shortest 1σ interval of the posterior for each parameter. These values are a useful reference. However, they conceal details about the probability of the these parameter values. Figure 5 shows a series of the two-dimensional posterior probability distributions for the seven free parameters in the fits. The expected covariance between parameters such as the impact parameter, b, and the relative size of the planet, $R_p/R_\star$, can be clearly seen. The MCMC chains are available for download such that these parameter dependencies can be properly accounted for in future statistical studies.

For 79 transit signals toward 36 cool KOIs there exist short cadence data. We follow the exact procedure outlined above for these data including preliminary fits and MCMC posterior sampling. These results are summarized in Table 2. The short cadence data fit for the same KOI shown in Figure 3, KOI-247.01, is shown in Figure 4 for reference. We note that the short cadence MCMC fits for KOI-1843.02, KOI-2036.03, and KOI-2704.03 failed due primarily to lack of sufficient data. These fits are included for completeness. However, the results from the long cadence fits should be used for further study.

4.2. Transit Timing Variations

4.2.1. TTV Search

For each transit signal, we use the best-fitting transit model to fit for the times of each transit event in search of potential TTVs (Agol et al. 2005; Holman & Murray 2005). A single parameter, Δt_0, quantifies the time deviation of mid-transit in relation to the expected time based on a linear ephemeris from the best fits. The model light curve is fit to each transit event letting only Δt_0 float using a Levenberg–Marquardt minimization (Markwardt 2009) to produce a list of observed-minus-calculated ($O-C$) values corresponding to each transit. Figure 6 shows an example of one of the known TTV planets in our sample, KOI-248.01.

To assess the significance of potential TTV signals, we first calculate the rms scatter in the times of mid-transit as estimated by the median absolute deviation σ_{O-C} and compare that to the median value of the estimated errors on the transit times $\bar{\sigma}_{\rm TT}$ (Mazeh et al. 2013). We consider values of $\sigma_O - C/\bar{\sigma}_{\rm TT} > 3.0$ to be significant. Next, we compute a Lomb Normalized Periodogram[9] for the calculated $O-C$ transit times. We calculate a p value for this peak by producing 10,000

[9] http://www.exelisvis.com/docs/LNP_TEST.html

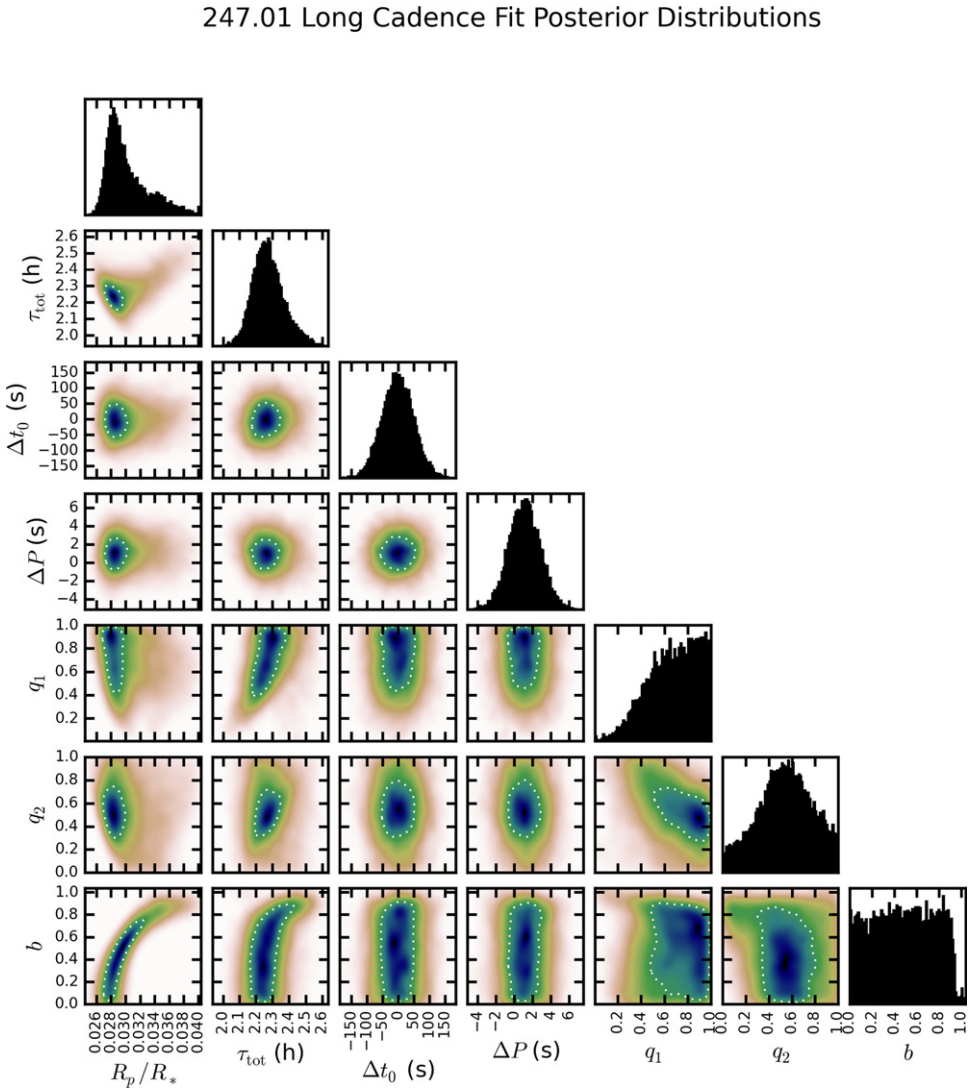

Figure 5. Array of 1D and 2D posteriors for the long cadence fit shown in Figure 3. The 2D posteriors were constructed using a 2D kernel density estimation that reveals covariances between parameters, most notably for R_p/R_*, b, and $\tau_{\rm tot}$. The 68.3% confidence contour for each 2D posterior is designated with a dotted white line.

(The complete figure set (163 images) is available.)

periodograms for the $O-C$ data randomly scrambled. The fractional number of periodogram peaks in the simulation that are greater than or equal to the original peak is interpreted as the probability that the measured periodogram is due to random noise, $p_{\rm LNP}$. This probability value is considered to be significant when $p_{\rm LNP} \leqslant 0.001$.

Finally, we fit both a sine curve and a polynomial to the $O-C$ data. The sine curve model contains an amplitude, period, phase, and offset. The starting parameters for the fit are a one minute amplitude, a period equal to the location of the peak of the periodogram, and zero phase and offset. To assess the significance of the fit results for the polynomial and sine curve models, we perform an F test on the fitted parameters by comparing the χ^2 values and degrees of freedom from a single parameter fit (a mean) and the polynomial or sine model. We again consider $p_{\rm sine} \leqslant 0.001$ and $p_{\rm poly} \leqslant 0.001$ to be significant.

4.2.2. TTV Results

The results were scrutinized by eye to weed out TTV signals due to stroboscopic effects and other, non-dynamical processes (Szabó et al. 2013). The results from our TTV search are summarized in Table 3. We recover 12 KOIs with significant TTV signals, 11 of which are in multi-transiting systems. These 12 planet candidates comprise 7.4% of the full M dwarf planet candidate sample and are found toward 7 of the 104, or 6.7% of all M dwarf KOIs. All of our TTV detections have been detected previously and are reported in the literature (Wu & Lithwick 2013; Mazeh et al. 2013; Kipping et al. 2014). However, these new transit timing results use only data from the *Kepler* mission. Following are a few notes regarding our TTV search.

KOI-3284 is reported to have a significant TTV signal by Kipping et al. (2014). Our tests show a signal at a period of ~190 days in both the periodogram and the sinusoid fit. However, the false alarm probability of the periodogram peak is found to be very high and this KOI also failed our F test for the sinusoidal fit. Therefore, we do not include this planet candidate in our list. KOI-2306 has $\sigma_{O-C}/\bar{\sigma_{\rm TT}} = 3.12$ due to the under sampling of the transit by the long cadence data, and we therefore exclude it. KOI-1907 and KOI-2130 show some signs of long period TTV signals at ~700 and ~1100 day

periods, respectively. However, both of these signals fall narrowly below our selection criteria and are therefore excluded.

KOI-952.02 is not reported by Mazeh et al. (2013) as a significant TTV source. However, we find that in 17 quarters of data the periodicity at ∼260 days is significant. This matches the period reported by Fabrycky et al. (2012). KOI-952.01 does not produce a signal significant enough to warrant inclusion in our list, although we do find that the first eight quarters of data are consistent with the results of Fabrycky et al. (2012), and a period of ∼260 days is apparent in our periodogram as the second highest peak but with a high formal false positive probability (FPP).

4.2.3. Fitting Transit Signals with TTVs

Transit timing variations can significantly affect the perceived transit shape under the assumption of a linear ephemeris. The effect essentially smears out the ingress and egress and potentially fills in the depth of the transit. The details depend on the exact nature of the TTVs. However, typically TTVs will bias the impact parameter to higher values, the transit duration to larger values, and the limb darkening parameters will tend toward values that produce a more severe contrast between the center of the star and the limb.

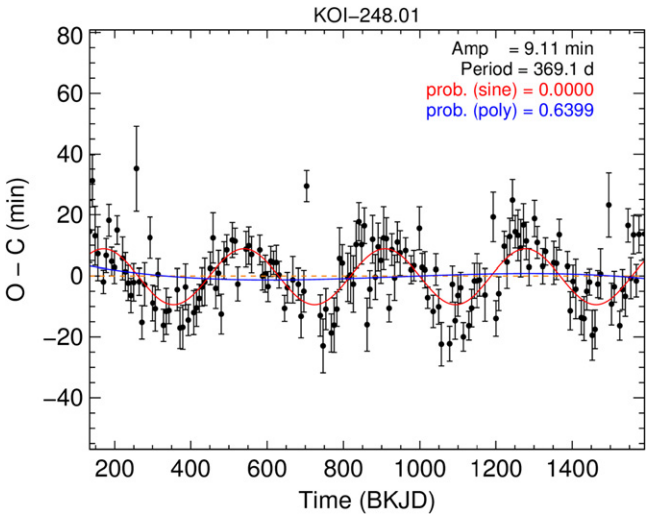

Figure 6. Transit timing variations (O–C) of KOI-248.01 fit with a pure sinusoid (red) and a polynomial (blue). These fits are only used to assess the significance of a potential TTV signal and are not used to fit the transits (see Section 4.2.3).

(The complete figure set (12 images) is available.)

Due to these effects, we refit the transit signals in our sample that show significant TTVs after folding on the individual transit times derived above. We first reject any individual transits that have mid-transit time errors that are either ill defined or more than 2σ from the median error. We then perform a transit fit using the same model outlined in Section 4, except that instead of fitting the period and mid-transit time, we fix the individual transit times.

We choose a large TTV source, KOI-886.01, as an example showing the potential effects of fitting a linear transit model to a planet that displays significant TTVs. The ∼2 hr peak-to-peak TTVs for KOI-886.01 bias the fits toward a larger impact parameter, a smaller planet, and a longer duration. The median posterior values for the impact parameter and relative planet size are discrepant at the 0.3 and 1.2σ levels. However the derived transit durations are in disagreement with 98% confidence. These results are shown in Figure 7.

5. FALSE POSITIVE PROBABILITY

The *Kepler* pipeline is known to have produced a high-fidelity sample of transiting exoplanets (Wu et al. 2010; Morton & Johnson 2011; Morton 2012; Christiansen et al. 2013; Fressin et al. 2013). Up to this point, we have treated every signal as a transiting exoplanet. However, it is prudent to assign to each transit signal a probability that the signal was generated from another astrophysical scenario. We use the methods of Morton & Johnson (2011) and Morton (2012) to analyze the light curves shapes that we have extracted to assign an FPP of each transit signal independently.

These FPPs are reported in Table 4 along with the probability of the transiting planet scenario compared to all other astrophysical scenarios, $P = L_{\rm TP}/L_{\rm FP}$; the specific occurrence assumed in the calculation, $f_{\rm pl,specific}$; and the specific planet occurrence needed to achieve a threshold FPP of 0.005, $f_{p,V}$. Included in each calculation is also a confusion radius within which false positives are permitted to exist. For this

Table 3
M Dwarf Planets with Transit Timing Variations

KOI	N	$\sigma_{O-C}/\bar{\sigma}_{\rm TT}$	LNP Amp.	$p_{\rm LNP}$	Sine Amp. (minutes)	$P_{\rm TTV}$ (days)	$p_{\rm sine}$	$p_{\rm poly}$
248.01	159	**2.19**	29.15	**0.0001**	9.71	365.97	**0.00000**	0.68916
248.02	100	**2.08**	7.25	**0.0009**	15.06	365.76	0.00383	0.42931
250.01	95	1.86	22.62	**0.0001**	9.76	743.74	**0.00000**	0.03606
250.02	52	1.63	9.38	**0.0009**	7.60	809.02	**0.00007**	0.18420
314.01	71	1.85	12.29	**0.0001**	5.46	1111.01	**0.00000**	**0.00000**
314.02	50	1.88	14.91	**0.0001**	13.86	1022.36	**0.00000**	**0.00000**
314.03	117	1.56	5.93	0.2357	32.43	1402.62	**0.00008**	**0.00031**
463.01	59	1.32	9.28	0.0021	3.65	314.51	**0.00025**	0.94999
886.01	158	1.82	43.24	**0.0001**	57.79	818.59	**0.00000**	0.06058
886.02	99	1.66	22.35	**0.0001**	105.95	871.50	**0.00000**	0.00706
898.01	123	0.89	7.37	0.0579	7.37	334.12	**0.00060**	0.86390
952.02	103	1.15	11.27	**0.0001**	17.61	261.62	**0.00012**	0.13167

Notes. Entries in boldface denote statistically significant values in our search for TTV signals (see text).

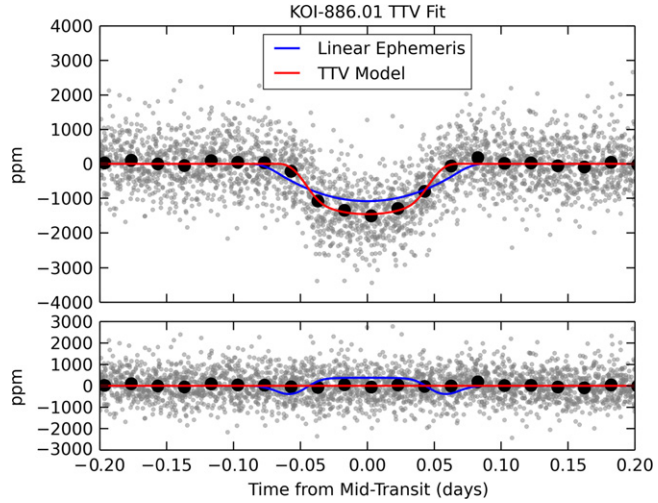

Figure 7. (Top) Long cadence *Kepler* photometry of KOI-886.01 phase folded on the transit times derived in Section 4.2. The best-fit model assuming a linear ephemeris is shown in blue and the best-fit model for the data folded on the non-linear transit times is shown in red. (Bottom) The residuals of the best-fit non-linear model. The difference between the linear and non-linear models is shown in blue. Assuming a linear ephemeris for this target which shows peak-to-peak TTVs of ∼2 hr significantly affects the derived transit parameters, in particular, the transit duration.

radius, we use three times the uncertainty in the multi-quarter difference-image pixel response function (PRF) fit reported in the Exoplanet Archive [the "PRF $\Delta\theta_{\rm MQ}$ (OOT)" column]. The minimum exclusion radius we allow is 0.5 arcsec, and the default value we use if no value is available is 4 arcsec. An example of a diagnostic plot generated by the FPP analysis is shown in Figure 8.

We find that 11% of the sample, or 18 of the 163, has a FPP of larger than 10%, consistent with estimates for the entire *Kepler* sample (Morton & Johnson 2011; Fressin et al. 2013). However, six of these high FPP targets are either known planets in the literature (e.g., KOI-254.01, Johnson et al. 2011b; KOI-886.02, Steffen et al. 2013; and KOI-1422.05, Rowe et al. 2014) or are part of three or four transit systems much less likely to be a false positives. Therefore, this is a high-fidelity sample of transiting exoplanets around the lowest-mass stars observed by the *Kepler* primary mission.

We do note that our treatment of exclusion radius ignores the possibility of more distant PRF contamination, as detected via the period-epoch match study of Coughlin et al. (2014), which found that "parent" eclipsing stars even up to 10–100 arcsec from the target star were able to cause "child" false positive signals. While that work discovered over 600 false positive KOIs, it also highlighted the possibility of further distant contaminants that might remain undetected because the "parent" may not be a known eclipsing system.

In order to estimate the rough probability of any of the present KOIs being false positives via this mechanism, we can use the numbers discussed by Coughlin et al. (2014). That work identified 12% of all known KOIs (not all planet candidates) to be due to PRF contamination. However, they pointed out that only about 1/3 of the stars in the *Kepler* field were downloaded, and so it might be reasonable to assume that for every discovered PRF contaminant, there might be two undiscovered, bringing the overall rate to about 36%. According to this reasoning, about 24% of all KOIs might be PRF contaminants that cannot be discovered by the period-epoch match method.

Table 4
False Positive Probability Results

KOI	FPP	P	$f_{p,\rm specific}$	$f_{p,V}$
247.01	0.0165	215	0.276	0.92400
248.01[a,b]	0.0000	290321	0.218	0.00069
248.02[a,b]	0.0902	39	0.258	5.08000
248.03[b]	0.0004	8541	0.276	0.02330
248.04[b]	0.0018	1998	0.276	0.09960
249.01	0.0000	848734	0.269	0.00023
250.01[a,b]	0.0940	64	0.149	3.08000
250.02[a,b]	0.0069	707	0.202	0.28200
250.03[b]	0.0003	10975	0.276	0.01820
250.04[b]	0.0030	1432	0.229	0.13900
251.01[b]	0.0003	17497	0.195	0.01140
251.02[b]	0.0036	997	0.276	0.20000
252.01	0.0018	2685	0.202	0.07400
253.01[b]	0.0122	428	0.189	0.46500
253.02[b]	0.0012	3041	0.276	0.06570
254.01	**0.3690**	171	0.010	1.20000
255.01[b]	0.0011	4614	0.195	0.04320
255.02[b]	0.0213	166	0.276	1.20000
314.01[a,b]	0.0000	162471	0.276	0.00123
314.02[a,b]	0.0000	86675	0.276	0.00230
314.03[a,b]	0.0069	520	0.276	0.38300
463.01[a]	0.0000	842598	0.276	0.00024
478.01	0.0000	91416	0.226	0.00218
531.01	**0.4820**	23	0.046	8.49000
571.01[b]	0.0002	14547	0.276	0.01370
571.02[b]	0.0000	241542	0.276	0.00082
571.03[b]	0.0000	88366	0.276	0.00226
571.04[b]	0.0014	2495	0.276	0.08000
571.05[b]	0.0046	787	0.276	0.25300
596.01	0.0000	355210	0.276	0.00056
641.01	0.0026	1406	0.276	0.14200
739.01	0.0001	54976	0.276	0.00363
781.01	0.0104	511	0.186	0.39000
812.01[b]	0.0000	117784	0.227	0.00169
812.02[b]	0.0001	64936	0.238	0.00307
812.03[b]	0.0001	50413	0.241	0.00395
812.04[b]	0.0098	366	0.276	0.54400
817.01[b]	0.0003	15136	0.258	0.01320
817.02[b]	0.0136	262	0.276	0.75700
818.01	0.0001	29391	0.233	0.00677
854.01	0.0002	22853	0.250	0.00871
886.01[a,b]	0.0269	136	0.265	1.46000
886.02[a,b]	**1.0000**	0	0.276	Inf
886.03[b]	0.0109	328	0.276	0.60700
898.01[a,b]	0.0001	49290	0.207	0.00404
898.02[b]	0.0000	154069	0.266	0.00129
898.03[b]	0.0004	11540	0.244	0.01720
899.01[b]	0.0000	128024	0.276	0.00155
899.02[b]	0.0001	32059	0.276	0.00622
899.03[b]	0.0001	38377	0.276	0.00519
936.01[b]	0.0000	412281	0.231	0.00048
936.02[b]	0.0000	126681	0.276	0.00157
947.01	0.0000	578234	0.251	0.00034
952.01[b]	0.0006	6507	0.243	0.03060
952.02[a,b]	0.0268	145	0.249	1.36000
952.03[b]	0.0012	3900	0.217	0.05100
952.04[b]	0.0141	253	0.276	0.78400
952.05[b]	0.0240	147	0.276	1.35000
961.01[b]	0.0119	300	0.276	0.66200
961.02[b]	0.0052	691	0.276	0.28800
961.03[b]	0.0424	81	0.276	2.44000
1078.01[b]	0.0000	102712	0.266	0.00194
1078.02[b]	0.0019	2155	0.249	0.09260
1078.03[b]	0.0046	881	0.247	0.22500

Table 4
(Continued)

KOI	FPP	P	$f_{p,\mathrm{specific}}$	$f_{p,V}$
1085.01	0.0011	3414	0.276	0.05830
1141.01	0.0002	16390	0.276	0.01210
1146.01	0.0028	1272	0.276	0.15700
1201.01	0.0024	1499	0.276	0.13300
1393.01	0.0150	290	0.226	0.68500
1397.01	0.0058	712	0.242	0.28000
1408.01	0.0025	1445	0.276	0.13800
1422.01[b]	0.0000	118789	0.276	0.00168
1422.02[b]	0.0001	35517	0.276	0.00561
1422.03[b]	0.0051	701	0.276	0.28400
1422.04[b]	0.0061	592	0.276	0.33600
1422.05[b]	**0.1740**	17	0.276	11.60000
1427.01	0.0001	31230	0.276	0.00640
1649.01	**0.1800**	16	0.276	12.10000
1681.01[b]	**0.7360**	1	0.276	153.00000
1681.02[b]	0.0089	403	0.276	0.49300
1681.03[b]	0.0182	195	0.276	1.02000
1702.01	0.0073	491	0.276	0.40600
1725.01	0.0007	5536	0.271	0.03590
1843.01[b]	0.0181	196	0.276	1.01000
1843.02[b]	0.0122	293	0.276	0.67700
1867.01[b]	0.0047	770	0.276	0.25900
1867.02[b]	0.0155	233	0.272	0.85500
1867.03[b]	0.0024	1493	0.276	0.13400
1868.01	0.0020	1994	0.249	0.09990
1879.01	0.0782	90	0.130	2.19000
1880.01	0.0009	4071	0.276	0.04890
1902.01	**0.9340**	0	0.254	719.00000
1907.01	0.0005	8143	0.268	0.02440
2006.01	0.0017	2153	0.276	0.09230
2036.01[b]	0.0336	104	0.276	1.91000
2036.02[b]	0.0215	164	0.276	1.21000
2057.01	0.0086	419	0.276	0.47500
2058.01	0.0032	1121	0.276	0.17700
2090.01	0.0036	1043	0.266	0.19100
2130.01	0.0045	846	0.262	0.23500
2156.01	0.0732	48	0.260	4.08000
2179.01[b]	0.0023	1592	0.270	0.12500
2179.02[b]	0.0281	125	0.276	1.59000
2191.01	**0.1180**	27	0.276	7.38000
2238.01	0.0069	522	0.276	0.38100
2306.01	0.0107	334	0.276	0.59500
2329.01	**0.1120**	28	0.276	6.93000
2347.01	0.0063	572	0.276	0.34800
2417.01	**0.1860**	15	0.276	12.50000
2418.01	0.0125	286	0.276	0.69600
2453.01	0.0267	132	0.276	1.51000
2480.01	0.0878	37	0.276	5.30000
2542.01	0.0079	455	0.276	0.43700
2626.01	0.0392	88	0.276	2.24000
2650.01[b]	0.0072	501	0.276	0.39700
2650.02[b]	0.0703	47	0.276	4.16000
2662.01	0.0071	504	0.276	0.39500
2704.01[b]	0.0011	5920	0.148	0.03360
2704.02[b]	0.0014	2814	0.259	0.07030
2704.03[b]	**0.9600**	0	0.276	1320.00000
2705.01	0.0001	26834	0.276	0.00741
2715.01[b]	0.0562	218	0.077	0.91700
2715.02[b]	0.0089	486	0.228	0.40900
2715.03[b]	0.0071	572	0.244	0.34700
2764.01	0.0005	6583	0.276	0.03030
2793.01[b]	0.0009	4685	0.232	0.04250
2793.02[b]	0.0076	475	0.276	0.41900
2839.01	0.0011	3382	0.276	0.05890
2842.01[b]	0.0001	32059	0.276	0.00622
2842.02[b]	0.0177	201	0.276	0.99100
2842.03[b]	0.0005	6977	0.276	0.02850
2845.01	0.0002	19268	0.276	0.01030
2862.01	0.0193	184	0.275	1.07000
2926.01[b]	0.0005	10656	0.193	0.01860
2926.02[b]	0.0014	3188	0.232	0.06250
2926.03[b]	0.0049	1145	0.178	0.17400
2926.04[b]	0.0004	11417	0.206	0.01740
2992.01	**0.3460**	8	0.233	24.60000
3010.01	0.0026	1422	0.275	0.14000
3034.01	0.0039	935	0.276	0.21300
3094.01	0.0183	194	0.276	1.02000
3102.01	0.0214	165	0.276	1.20000
3119.01	0.0014	2495	0.276	0.07980
3140.01	**0.2620**	10	0.276	19.60000
3144.01	0.0007	5553	0.276	0.03590
3263.01	**0.7140**	16	0.024	11.80000
3282.01	0.0008	4860	0.243	0.04090
3284.01	0.0078	457	0.276	0.43500
3414.01	**0.9620**	13	0.003	17.30000
3444.01[b]	0.0046	777	0.276	0.25600
3444.02[b]	**0.4130**	6	0.211	29.60000
3444.03[b]	0.0370	94	0.276	2.11000
3444.04[b]	0.0416	83	0.276	2.38000
3497.01	0.0001	31230	0.276	0.00637
3749.01	**0.8550**	14	0.012	14.30000
4087.01	0.0004	8442	0.276	0.02360
4252.01	0.0124	288	0.276	0.69000
4290.01	0.0238	148	0.276	1.34000
4427.01	0.0636	54	0.268	3.62000
4875.01	0.0022	1635	0.276	0.12200
5228.01	**0.8530**	0	0.276	320.00000
5359.01	0.0006	6109	0.274	0.03260
5692.01	0.0124	288	0.276	0.68900

Notes. Entries in boldface denote False positive probabilities larger than 10%. These values are derived without consideration of the presence of TTV signals or other transit signals toward the same source.
[a] Source of significant TTV signal.
[b] Multi-transit candidate system.

However, they also go on to point out that 5/6 of the false positives they detected were also identified as false positives by other methods (e.g., pixel-centroid offsets, detected secondary eclipses, etc). So this implies that of those previously mentioned 24%, only 1/6 of those, or 4% of all KOIs, may be long-distance PRF contaminants undetected by any *Kepler* FP vetting procedure and thus achieving planet candidate status. Comparing this to the ~64% of all KOIs expected to be true planets, we estimate that an additional ~6–7% of *Kepler* planet candidates, beyond what we calculate here using the methods of Morton (2012), could still be false positives. Incorporating in detail this additional long-distance PRF contamination into quantitative models of false positive probability is thus warranted but beyond the scope of this present work.

In addition, we also note that the FPPs presented in this paper do not consider the number of independent transit signals in the light curve or the possibility of detected TTVs, both of

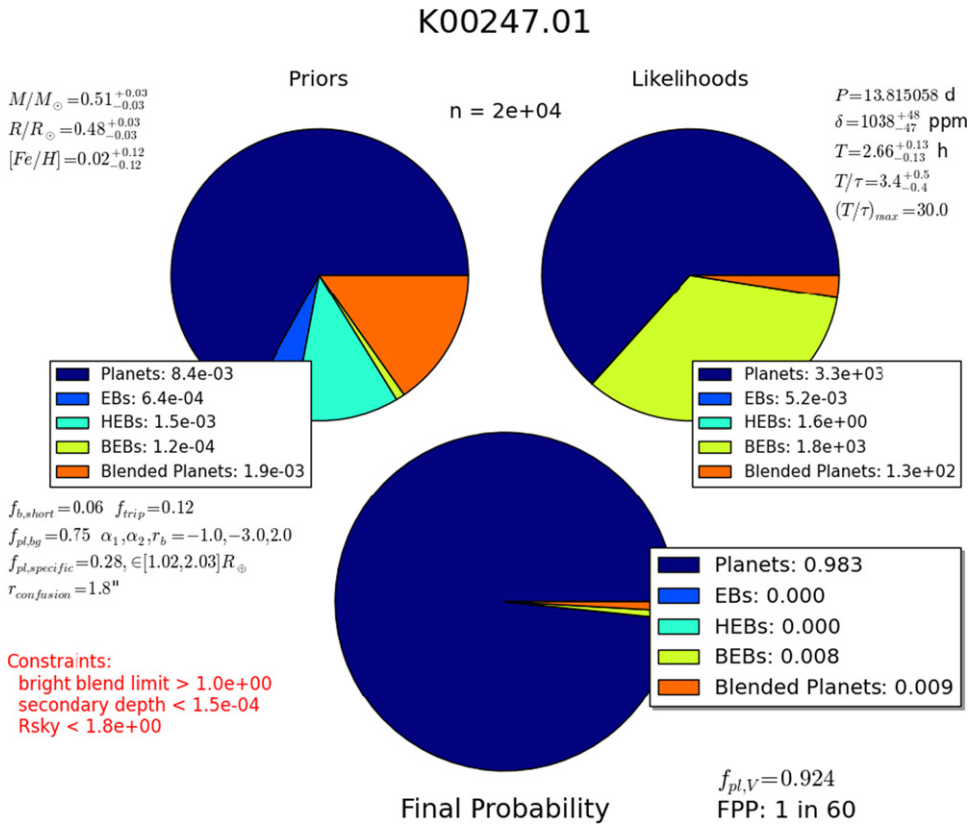

Figure 8. Diagnostic plot showing the key results of the false positive probability analysis for the sample of transiting planet cadidates around low-mass stars. The top left pie chart shows the prior likelihoods of the five different scenarios considered: transiting planet (Planets), eclipsing binary (EB), heirarchical eclipsing binary (HEB), background eclipsing binary (BEB), and blended planet. These fractions are calculated with a Galactic model in the direction of the target star with an assumed planet occurrence ($f_{\rm pl,specific}$). The top right is the likelihood of these different scenarios given the shape of the long cadence light curve. For this case, KOI-247.01, the signal is most likely a transit signal around the intended star. However, the most likely false positive scenarios are background eclipsing binaries and blended planet signals.

(The complete figure set (163 images) is available.)

which may substantially reduce the FPP (e.g., Ford et al. 2011; Lissauer et al. 2014; Rowe et al. 2014).

6. THE ENSEMBLE OF M DWARF PLANET CANDIDATES

The cool KOI catalog enables the study of the smallest and possibly most numerous planet population discovered by *Kepler* and helps to advance our knowledge of planet formation around the most common types of stars. It is estimated that 75% of the stars within 10 pc are M dwarfs (Henry et al. 1994, 2004; Reid & Cruz 2002). Therefore, by targeting this population we are also learning what can be expected of the closest planetary systems outside our solar system.

To further our understanding of this sample of small planets, we present uniformly derived transit parameters for all known transit signals around cool KOIs. These stars constitute a small fraction (about 2%) of the total *Kepler* targets. However, the sample is large enough to allow for meaningful statistical analyses (Ballard & Johnson 2014; Morton & Swift 2014). Since M dwarf stars are difficult to characterize observationally, it is also important that our sample be small enough such that each individual star can be addressed with followup observations.

The planet candidates of this work have been drawn from the Exoplanet Archive list using the cool dwarf photometric cuts of Mann et al. (2012). Additional vetting was performed using near-infrared, medium-resolution spectroscopy (Muirhead et al. 2012b, 2014). Our final sample contains 163 planets around 104 cool stars. The total number of single transit systems is 74; meanwhile, there are 12 double systems, 10 triple systems, 5 quadruple systems, and 3 quintuple systems. A total of 54.6% of these planets are found in multi-transit systems, and 12.4% of these multis show significant TTV signals. On the contrary, only one single transit system out of 74, or 1.4%, shows a significant TTV signal.

The final results of our transit fits to the *Kepler* long and short cadence data are summarized in Tables 1 and 2, respectively. These tables display the results from the linear ephemeris model for all KOIs except those listed in Table 3. For those sources we report the period, P, and mid-transit time, t_0, from the linear ephemeris fits (although it should be noted that these parameters are not strictly defined in this context) and the other transit parameters from the non-linear ephemeris fits. An earlier version of this catalog has already been used in the literature to infer the statistical properties of the *Kepler* M dwarf planet population (Morton & Swift 2014), and is presented here so that it may be used for further statistical studies. Each transit signal has been treated individually, and we have generated posterior samples of the seven transit parameters using uninformed priors that are available for download along with a suite of diagnostic plots for each KOI.

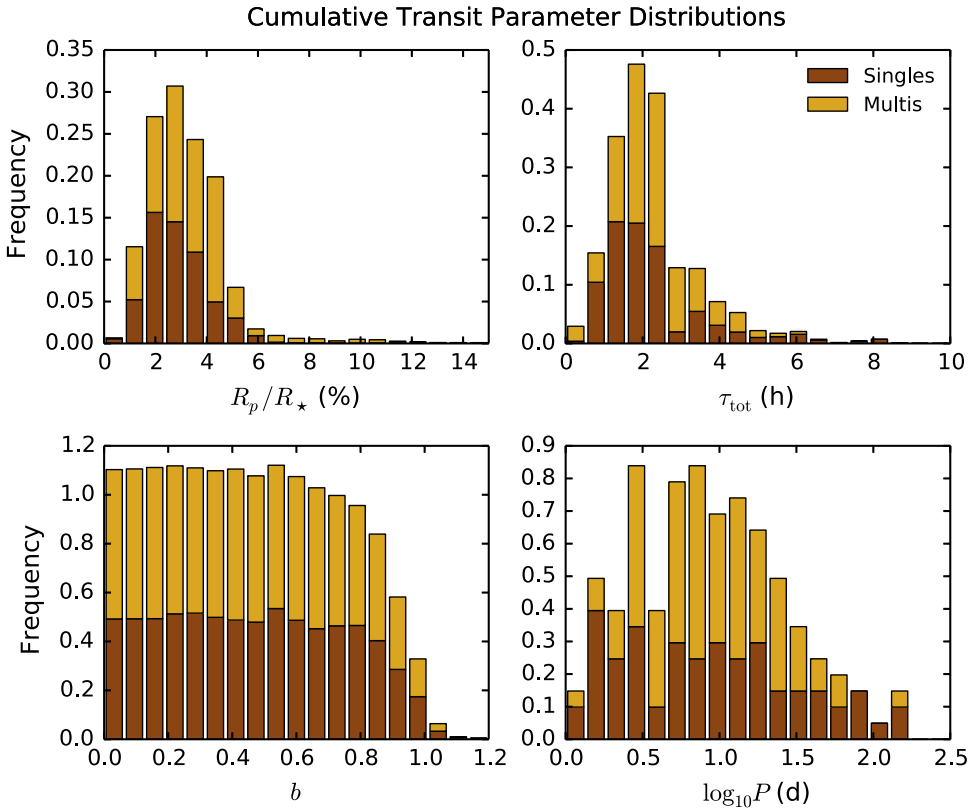

Figure 9. Cumulative distributions of four of the seven transit parameters for the sample of exoplanet candidates orbiting *Kepler*'s coolest dwarf stars. The radii of the planet candidates (top left) are displayed in terms of a percentage of the radius of the host star. The total duration (first to fourth contact point, top right) is shown in units of hours. The impact parameter (bottom left) is seen to be mostly indeterminable from the long cadence data, except for KOI-254/*Kepler*-45 which accounts for the bump near $b = 0.54$. The periods of the planet candidates span more than two orders of magnitude and are shown on a $\log_{10}$ scale (bottom right) to reveal further details of the distribution. The stacked histograms differentiate the sample of single transit systems (brown) and planets in multi-transit systems (gold).

Table 5
M Star *Kepler* Objects of Interest

KOI	KIC	$N_{\rm pl}$	Mass ($M_\odot$)	Radius ($R_\odot$)	$T_{\rm eff}$ (K)	[Fe/H] (dex)	Ref.	$P_{\rm rot}$ (days)	K_p	J	K_s
247	11852982	1	$0.51^{+0.03}_{-0.03}$	$0.48^{+0.03}_{-0.03}$	3735^{+49}_{-33}	$0.02^{+0.12}_{-0.12}$	1	16.2	14.22	12.01	11.12
248	5364071	4	$0.55^{+0.04}_{-0.04}$	$0.52^{+0.04}_{-0.04}$	3838^{+111}_{-74}	$-0.02^{+0.14}_{-0.14}$	1	18.3	15.26	13.18	12.38
249	9390653	1	$0.40^{+0.05}_{-0.05}$	$0.39^{+0.04}_{-0.04}$	3562^{+50}_{-64}	$-0.13^{+0.13}_{-0.13}$	1	43.6	14.49	12.00	11.15
250	9757613	4	$0.55^{+0.05}_{-0.05}$	$0.52^{+0.05}_{-0.05}$	3884^{+199}_{-27}	$-0.13^{+0.13}_{-0.13}$	1	17.8	15.47	13.41	12.63
251	10489206	2	$0.53^{+0.03}_{-0.03}$	$0.50^{+0.03}_{-0.03}$	3811^{+48}_{-71}	$-0.06^{+0.11}_{-0.11}$	1	14.5	14.75	12.48	11.68
252	11187837	1	$0.52^{+0.03}_{-0.03}$	$0.49^{+0.03}_{-0.03}$	3745^{+70}_{-56}	$0.06^{+0.11}_{-0.11}$	1	39.5	15.61	13.42	12.55
253	11752906	2	$0.59^{+0.04}_{-0.04}$	$0.56^{+0.04}_{-0.04}$	3759^{+182}_{-34}	$0.49^{+0.14}_{-0.14}$	1	⋯	15.25	13.09	12.29
254	5794240	1	$0.58^{+0.03}_{-0.03}$	$0.55^{+0.03}_{-0.03}$	3793^{+133}_{-34}	$0.32^{+0.13}_{-0.13}$	1	15.8	15.98	13.75	12.89
255	7021681	2	$0.53^{+0.04}_{-0.04}$	$0.51^{+0.04}_{-0.04}$	3780^{+68}_{-73}	$-0.01^{+0.15}_{-0.15}$	1	⋯	15.11	12.91	12.08
314	7603200	3	$0.52^{+0.03}_{-0.03}$	$0.49^{+0.03}_{-0.03}$	3847^{+46}_{-59}	$-0.25^{+0.12}_{-0.12}$	1	19.4	12.93	10.29	9.51
463	8845205	1	$0.26^{+0.05}_{-0.05}$	$0.26^{+0.04}_{-0.04}$	3389^{+57}_{-48}	$-0.12^{+0.13}_{-0.13}$	1	50.8	14.71	12.27	11.45
478	10990886	1	$0.54^{+0.03}_{-0.03}$	$0.51^{+0.03}_{-0.03}$	3744^{+23}_{-92}	$0.19^{+0.12}_{-0.12}$	1	34.2	14.27	11.80	10.96
531	10395543	1	$0.61^{+0.04}_{-0.04}$	$0.59^{+0.04}_{-0.04}$	4004^{+120}_{-172}	$0.11^{+0.14}_{-0.14}$	1	46.8	14.42	12.36	11.61
571	8120608	5	$0.48^{+0.03}_{-0.03}$	$0.45^{+0.03}_{-0.03}$	3748^{+90}_{-20}	$-0.34^{+0.12}_{-0.12}$	1	34.3	14.62	12.47	11.60
596	10388286	1	$0.49^{+0.03}_{-0.03}$	$0.46^{+0.03}_{-0.03}$	3670^{+53}_{-53}	$0.01^{+0.11}_{-0.11}$	1	37.5	14.82	12.44	11.57
641	5131180	1	$0.27^{+0.05}_{-0.05}$	$0.28^{+0.05}_{-0.05}$	3391^{+50}_{-50}	$-0.10^{+0.10}_{-0.10}$	2	⋯	13.58	11.52	10.70
739	10386984	1	$0.52^{+0.04}_{-0.04}$	$0.50^{+0.04}_{-0.04}$	3733^{+91}_{-47}	$0.11^{+0.15}_{-0.15}$	1	39.6	15.49	13.44	12.63
781	11923270	1	$0.50^{+0.04}_{-0.04}$	$0.47^{+0.04}_{-0.04}$	3691^{+65}_{-89}	$-0.00^{+0.14}_{-0.14}$	1	36.4	15.94	13.47	12.63
812	4139816	4	$0.53^{+0.05}_{-0.05}$	$0.51^{+0.05}_{-0.05}$	3949^{+131}_{-130}	$-0.45^{+0.14}_{-0.14}$	1	15.0	15.95	13.95	13.11
817	4725681	2	$0.53^{+0.03}_{-0.03}$	$0.51^{+0.03}_{-0.03}$	3747^{+81}_{-40}	$0.11^{+0.12}_{-0.12}$	1	15.4	15.41	13.22	12.31
818	4913852	1	$0.54^{+0.04}_{-0.04}$	$0.51^{+0.04}_{-0.04}$	3698^{+34}_{-112}	$0.28^{+0.16}_{-0.16}$	1	34.3	15.88	13.40	12.49
854	6435936	1	$0.49^{+0.04}_{-0.04}$	$0.46^{+0.04}_{-0.04}$	3593^{+37}_{-65}	$0.25^{+0.15}_{-0.15}$	1	20.2	15.85	13.44	12.53
886	7455287	3	$0.48^{+0.04}_{-0.04}$	$0.46^{+0.04}_{-0.04}$	3712^{+57}_{-69}	$-0.13^{+0.14}_{-0.14}$	1	34.6	15.85	13.51	12.65
898	7870390	3	$0.53^{+0.04}_{-0.04}$	$0.51^{+0.04}_{-0.04}$	3907^{+80}_{-104}	$-0.33^{+0.13}_{-0.13}$	1	22.1	15.78	13.74	12.95

Table 5
(Continued)

KOI	KIC	N_{pl}	Mass ($M_\odot$)	Radius ($R_\odot$)	T_{eff} (K)	[Fe/H] (dex)	Ref.	P_{rot} (days)	K_p	J	K_s
899	7907423	3	$0.43^{+0.04}_{-0.04}$	$0.41^{+0.04}_{-0.04}$	3565^{+47}_{-48}	$0.01^{+0.11}_{-0.11}$	1	36.1	15.23	12.84	11.97
936	9388479	2	$0.47^{+0.04}_{-0.04}$	$0.45^{+0.04}_{-0.04}$	3582^{+61}_{-44}	$0.19^{+0.13}_{-0.13}$	1	36.0	15.07	12.60	11.72
947	9710326	1	$0.49^{+0.04}_{-0.04}$	$0.47^{+0.04}_{-0.04}$	3753^{+54}_{-98}	$-0.26^{+0.13}_{-0.13}$	1	25.2	15.19	12.91	12.10
952	9787239	5	$0.51^{+0.04}_{-0.04}$	$0.48^{+0.04}_{-0.04}$	3731^{+71}_{-73}	$-0.02^{+0.13}_{-0.13}$	1	37.1	15.80	13.61	12.76
961	8561063	3	$0.13^{+0.05}_{-0.05}$	$0.17^{+0.04}_{-0.04}$	3204^{+61}_{-40}	$-0.48^{+0.12}_{-0.12}$	1	⋯	15.92	12.18	11.47
1078	10166274	3	$0.49^{+0.05}_{-0.05}$	$0.46^{+0.04}_{-0.04}$	3783^{+109}_{-82}	$-0.34^{+0.17}_{-0.17}$	1	22.4	15.44	13.33	12.48
1085	10118816	1	$0.55^{+0.05}_{-0.05}$	$0.53^{+0.05}_{-0.05}$	3979^{+257}_{-78}	$-0.33^{+0.13}_{-0.13}$	1	39.7	15.23	13.03	12.25
1141	8346392	1	$0.58^{+0.07}_{-0.07}$	$0.55^{+0.06}_{-0.06}$	3968^{+425}_{-69}	$-0.14^{+0.12}_{-0.12}$	1	17.9	15.95	13.88	13.05
1146	8351704	1	$0.39^{+0.05}_{-0.05}$	$0.37^{+0.04}_{-0.04}$	3560^{+62}_{-39}	$-0.18^{+0.13}_{-0.13}$	1	25.6	15.65	13.44	12.61
1201	4061149	1	$0.47^{+0.03}_{-0.03}$	$0.45^{+0.03}_{-0.03}$	3697^{+82}_{-45}	$-0.19^{+0.14}_{-0.14}$	1	28.8	15.60	13.41	12.61
1393	9202151	1	$0.57^{+0.06}_{-0.05}$	$0.56^{+0.08}_{-0.05}$	3872^{+101}_{-50}	$0.00^{+0.10}_{-0.10}$	2	⋯	15.80	13.62	12.77
1397	9427402	1	$0.52^{+0.06}_{-0.06}$	$0.49^{+0.06}_{-0.06}$	3822^{+169}_{-51}	$-0.24^{+0.15}_{-0.15}$	1	⋯	15.37	13.25	12.43
1408	9150827	2	$0.57^{+0.03}_{-0.03}$	$0.54^{+0.03}_{-0.03}$	3955^{+95}_{-82}	$-0.16^{+0.12}_{-0.12}$	1	25.0	14.69	12.66	11.81
1422	11497958	5	$0.39^{+0.05}_{-0.05}$	$0.37^{+0.04}_{-0.04}$	3522^{+76}_{-49}	$-0.08^{+0.12}_{-0.12}$	1	35.6	15.92	13.39	12.60
1427	11129738	1	$0.54^{+0.04}_{-0.04}$	$0.51^{+0.04}_{-0.04}$	3880^{+141}_{-75}	$-0.24^{+0.14}_{-0.14}$	1	33.8	15.84	13.80	13.06
1649	11337141	1	$0.58^{+0.06}_{-0.06}$	$0.55^{+0.05}_{-0.05}$	3877^{+156}_{-89}	$0.09^{+0.13}_{-0.13}$	1	25.6	14.96	12.64	11.79
1681	5531953	3	$0.46^{+0.04}_{-0.04}$	$0.43^{+0.04}_{-0.04}$	3657^{+70}_{-64}	$-0.12^{+0.14}_{-0.14}$	1	24.5	15.85	13.46	12.58
1702	7304449	1	$0.26^{+0.05}_{-0.05}$	$0.27^{+0.04}_{-0.04}$	3356^{+74}_{-57}	$-0.06^{+0.14}_{-0.14}$	1	45.9	15.72	12.99	12.20
1725	10905746	1	$0.44^{+0.04}_{-0.04}$	$0.42^{+0.04}_{-0.04}$	3618^{+57}_{-41}	$-0.06^{+0.12}_{-0.12}$	1	18.2	13.50	10.65	9.80
1843	5080636	2	$0.54^{+0.04}_{-0.04}$	$0.51^{+0.04}_{-0.04}$	3705^{+37}_{-81}	$0.27^{+0.12}_{-0.12}$	1	34.3	14.40	11.95	11.06
1867	8167996	3	$0.51^{+0.04}_{-0.04}$	$0.48^{+0.04}_{-0.04}$	3717^{+123}_{-36}	$0.03^{+0.16}_{-0.16}$	1	24.8	15.02	12.79	11.95
1868	6773862	1	$0.55^{+0.06}_{-0.06}$	$0.52^{+0.06}_{-0.06}$	3828^{+134}_{-82}	$-0.05^{+0.13}_{-0.13}$	1	25.0	15.22	13.14	12.29
1879	8367644	1	$0.59^{+0.09}_{-0.09}$	$0.56^{+0.08}_{-0.08}$	3829^{+324}_{-73}	$0.31^{+0.16}_{-0.16}$	1	21.9	15.97	13.59	12.73
1880	10332883	1	$0.57^{+0.05}_{-0.05}$	$0.54^{+0.05}_{-0.05}$	3950^{+60}_{-178}	$-0.15^{+0.14}_{-0.14}$	1	18.9	14.44	12.26	11.45
1902	5809954	1	$0.46^{+0.05}_{-0.05}$	$0.44^{+0.04}_{-0.04}$	3647^{+69}_{-86}	$-0.08^{+0.14}_{-0.14}$	1	⋯	14.65	12.29	11.45
1907	7094486	1	$0.51^{+0.05}_{-0.05}$	$0.48^{+0.05}_{-0.05}$	3594^{+113}_{-25}	$0.39^{+0.18}_{-0.18}$	1	18.2	15.28	13.19	12.35
2006	10525027	1	$0.52^{+0.03}_{-0.03}$	$0.49^{+0.03}_{-0.03}$	3756^{+80}_{-59}	$0.01^{+0.14}_{-0.14}$	1	28.8	14.22	11.97	11.18
2036	6382217	2	$0.55^{+0.06}_{-0.06}$	$0.52^{+0.05}_{-0.05}$	3758^{+281}_{-2}	$0.19^{+0.13}_{-0.13}$	1	32.1	15.77	13.60	12.81
2057	9573685	1	$0.59^{+0.06}_{-0.06}$	$0.56^{+0.06}_{-0.06}$	3974^{+182}_{-188}	$-0.05^{+0.16}_{-0.16}$	1	30.2	15.03	12.88	12.07
2058	10329835	1	$0.52^{+0.04}_{-0.04}$	$0.49^{+0.04}_{-0.04}$	3747^{+144}_{-50}	$-0.00^{+0.15}_{-0.15}$	1	22.2	15.31	13.22	12.41
2090	11348997	1	$0.60^{+0.09}_{-0.09}$	$0.57^{+0.08}_{-0.08}$	3889^{+522}_{-141}	$0.32^{+0.15}_{-0.15}$	1	36.5	15.53	13.26	12.39
2130	2161536	1	$0.59^{+0.06}_{-0.06}$	$0.56^{+0.05}_{-0.05}$	3967^{+206}_{-137}	$0.06^{+0.15}_{-0.15}$	1	26.8	15.66	13.59	12.77
2156	2556650	1	$0.49^{+0.05}_{-0.05}$	$0.47^{+0.04}_{-0.04}$	3754^{+108}_{-42}	$-0.26^{+0.16}_{-0.16}$	1	28.1	15.96	13.67	12.83
2179	10670119	2	$0.56^{+0.04}_{-0.04}$	$0.53^{+0.04}_{-0.04}$	3834^{+138}_{-67}	$0.05^{+0.13}_{-0.13}$	1	19.6	15.67	13.25	12.39
2191	5601258	1	$0.57^{+0.04}_{-0.04}$	$0.54^{+0.04}_{-0.04}$	3870^{+77}_{-102}	$0.10^{+0.13}_{-0.13}$	1	17.8	14.91	12.66	11.81
2238	8229458	1	$0.54^{+0.04}_{-0.04}$	$0.51^{+0.04}_{-0.04}$	3809^{+106}_{-90}	$-0.02^{+0.14}_{-0.14}$	1	14.9	14.63	12.49	11.68
2306	6666233	1	$0.57^{+0.07}_{-0.07}$	$0.54^{+0.06}_{-0.06}$	3861^{+292}_{-64}	$0.08^{+0.13}_{-0.13}$	1	24.9	14.78	12.63	11.83
2329	11192235	1	$0.51^{+0.05}_{-0.05}$	$0.49^{+0.05}_{-0.05}$	3823^{+138}_{-73}	$-0.28^{+0.17}_{-0.17}$	1	34.1	15.65	13.49	12.67
2347	8235924	1	$0.57^{+0.08}_{-0.08}$	$0.54^{+0.07}_{-0.07}$	3817^{+510}_{-46}	$0.24^{+0.13}_{-0.13}$	1	⋯	14.93	12.86	12.06
2417	9654468	1	$0.27^{+0.05}_{-0.05}$	$0.28^{+0.05}_{-0.05}$	3391^{+50}_{-50}	$-0.10^{+0.10}_{-0.10}$	2	21.3	16.22	14.12	13.43
2418	10027247	1	$0.43^{+0.05}_{-0.07}$	$0.41^{+0.05}_{-0.08}$	3724^{+60}_{-74}	$-0.40^{+0.10}_{-0.10}$	2	17.6	15.47	13.23	12.37
2453	8631751	1	$0.27^{+0.06}_{-0.06}$	$0.27^{+0.05}_{-0.05}$	3451^{+96}_{-51}	$-0.44^{+0.16}_{-0.16}$	1	⋯	15.63	13.19	12.42
2480	8189801	1	$0.55^{+0.07}_{-0.05}$	$0.55^{+0.09}_{-0.05}$	3990^{+84}_{-66}	$-0.20^{+0.30}_{-0.30}$	2	32.0	15.74	13.73	12.88
2542	6183511	1	$0.37^{+0.06}_{-0.06}$	$0.36^{+0.06}_{-0.06}$	3466^{+66}_{-70}	$0.10^{+0.15}_{-0.15}$	1	29.4	15.53	12.86	12.03
2626	11768142	1	$0.43^{+0.06}_{-0.06}$	$0.40^{+0.05}_{-0.05}$	3568^{+52}_{-105}	$-0.02^{+0.16}_{-0.16}$	1	⋯	15.93	13.45	12.63
2650	8890150	2	$0.52^{+0.04}_{-0.04}$	$0.50^{+0.04}_{-0.04}$	3765^{+96}_{-49}	$0.01^{+0.13}_{-0.13}$	1	19.9	15.99	13.82	12.95
2662	3426367	1	$0.48^{+0.05}_{-0.05}$	$0.46^{+0.05}_{-0.05}$	3628^{+57}_{-74}	$0.14^{+0.14}_{-0.14}$	1	34.0	14.49	11.88	11.02
2704	9730163	2	$0.24^{+0.06}_{-0.06}$	$0.26^{+0.05}_{-0.05}$	3267^{+70}_{-54}	$0.27^{+0.15}_{-0.15}$	1	⋯	17.48	13.54	12.61
2705	11453592	1	$0.39^{+0.05}_{-0.05}$	$0.38^{+0.05}_{-0.05}$	3494^{+55}_{-54}	$0.11^{+0.14}_{-0.14}$	1	⋯	14.72	11.57	10.73
2715	9837661	3	$0.50^{+0.08}_{-0.08}$	$0.47^{+0.07}_{-0.07}$	3640^{+291}_{-74}	$0.20^{+0.20}_{-0.20}$	1	41.3	16.83	14.83	13.88
2764	10073672	1	$0.59^{+0.11}_{-0.11}$	$0.57^{+0.11}_{-0.11}$	4045^{+***}_{-114}	$-0.16^{+0.16}_{-0.16}$	1	27.7	15.79	13.67	12.87
2793	9823519	2	$0.47^{+0.08}_{-0.05}$	$0.44^{+0.07}_{-0.05}$	3698^{+75}_{-50}	$-0.20^{+0.20}_{-0.20}$	2	19.0	16.28	13.99	13.12
2839	6186964	1	$0.58^{+0.08}_{-0.08}$	$0.55^{+0.08}_{-0.08}$	3943^{+178}_{-184}	$-0.05^{+0.17}_{-0.17}$	1	17.8	15.88	13.77	12.96
2842	8733898	3	$0.16^{+0.02}_{-0.02}$	$0.18^{+0.02}_{-0.02}$	3204^{+51}_{-57}	$-0.30^{+0.13}_{-0.13}$	1	⋯	16.26	13.59	12.83
2845	10591855	1	$0.72^{+0.11}_{-0.11}$	$0.67^{+0.11}_{-0.11}$	4342^{+712}_{-530}	$0.32^{+0.17}_{-0.17}$	1	29.1	15.57	13.51	12.70
2862	6679295	1	$0.52^{+0.06}_{-0.06}$	$0.50^{+0.06}_{-0.06}$	3679^{+146}_{-44}	$0.26^{+0.18}_{-0.18}$	1	17.7	15.91	13.66	12.76
2926	10122538	4	$0.60^{+0.09}_{-0.09}$	$0.57^{+0.09}_{-0.09}$	3899^{+717}_{-110}	$0.24^{+0.17}_{-0.17}$	1	24.0	16.28	14.22	13.34

Table 5
(Continued)

KOI	KIC	N_{pl}	Mass ($M_\odot$)	Radius ($R_\odot$)	T_{eff} (K)	[Fe/H] (dex)	Ref.	P_{rot} (days)	K_p	J	K_s
2992	8509442	1	$0.57^{+0.09}_{-0.05}$	$0.55^{+0.08}_{-0.05}$	3952^{+93}_{-55}	$-0.10^{+0.30}_{-0.30}$	2	15.0	15.99	13.91	13.04
3010	3642335	1	$0.53^{+0.09}_{-0.09}$	$0.51^{+0.08}_{-0.08}$	3810^{+54}_{-270}	$-0.03^{+0.24}_{-0.24}$	1	14.5	15.76	13.59	12.77
3034	2973386	1	$0.49^{+0.06}_{-0.06}$	$0.46^{+0.06}_{-0.06}$	3713^{+230}_{-44}	$-0.10^{+0.18}_{-0.18}$	1	37.2	15.57	13.45	12.61
3094	12352520	1	$0.53^{+0.05}_{-0.05}$	$0.50^{+0.05}_{-0.05}$	3805^{+68}_{-50}	$-0.10^{+0.10}_{-0.10}$	2	36.2	15.74	13.52	12.75
3102	9605552	1	$0.38^{+0.07}_{-0.11}$	$0.35^{+0.06}_{-0.12}$	3773^{+50}_{-134}	$-0.80^{+0.20}_{-0.20}$	2	31.0	15.98	13.86	13.10
3119	5551672	1	$0.22^{+0.07}_{-0.07}$	$0.23^{+0.06}_{-0.06}$	3371^{+75}_{-125}	$-0.40^{+0.21}_{-0.21}$	1	⋯	16.95	14.38	13.54
3140	5978170	1	$0.27^{+0.05}_{-0.05}$	$0.28^{+0.05}_{-0.05}$	3391^{+50}_{-50}	$-0.10^{+0.10}_{-0.10}$	2	15.2	15.56	13.52	12.77
3144	5688790	1	$0.45^{+0.05}_{-0.05}$	$0.42^{+0.05}_{-0.05}$	3679^{+67}_{-99}	$-0.31^{+0.18}_{-0.18}$	1	31.7	16.11	13.58	12.74
3263	11853130	1	$0.49^{+0.06}_{-0.06}$	$0.46^{+0.05}_{-0.05}$	3680^{+128}_{-78}	$0.00^{+0.17}_{-0.17}$	1	19.9	15.95	13.56	12.73
3282	12066569	1	$0.55^{+0.07}_{-0.07}$	$0.53^{+0.07}_{-0.07}$	3901^{+264}_{-106}	$-0.20^{+0.14}_{-0.14}$	1	18.0	15.85	13.77	12.92
3284	6497146	1	$0.55^{+0.04}_{-0.04}$	$0.52^{+0.04}_{-0.04}$	3748^{+35}_{-112}	$0.16^{+0.14}_{-0.14}$	1	36.5	14.47	12.13	11.20
3414	6023859	1	$0.56^{+0.09}_{-0.05}$	$0.54^{+0.09}_{-0.05}$	3900^{+140}_{-50}	$-0.10^{+0.20}_{-0.20}$	2	14.5	15.48	13.37	12.52
3444	5384713	4	$0.51^{+0.04}_{-0.04}$	$0.48^{+0.04}_{-0.04}$	3665^{+88}_{-82}	$0.16^{+0.14}_{-0.14}$	1	20.3	13.69	11.17	10.31
3497	8424002	1	$0.32^{+0.06}_{-0.06}$	$0.32^{+0.05}_{-0.05}$	3412^{+50}_{-106}	$0.02^{+0.17}_{-0.17}$	1	9.4	13.39	11.31	10.62
3749	11547869	1	$0.28^{+0.07}_{-0.07}$	$0.29^{+0.06}_{-0.06}$	3337^{+130}_{-55}	$0.10^{+0.18}_{-0.18}$	1	19.5	16.42	13.73	12.97
4087	6106282	1	$0.48^{+0.05}_{-0.07}$	$0.48^{+0.06}_{-0.06}$	3813^{+58}_{-87}	$-0.30^{+0.10}_{-0.10}$	2	17.5	15.13	12.96	12.12
4252	10525049	1	$0.58^{+0.06}_{-0.06}$	$0.55^{+0.06}_{-0.06}$	3873^{+275}_{-76}	$0.12^{+0.12}_{-0.12}$	1	30.9	13.98	11.70	10.87
4290	5868793	1	$0.18^{+0.04}_{-0.04}$	$0.20^{+0.04}_{-0.04}$	3187^{+78}_{-84}	$0.10^{+0.17}_{-0.17}$	1	⋯	17.06	13.28	12.44
4427	4172805	1	$0.53^{+0.06}_{-0.06}$	$0.50^{+0.06}_{-0.06}$	3813^{+272}_{-30}	$-0.07^{+0.14}_{-0.14}$	1	39.0	15.65	13.34	12.50
4875	2986833	1	$0.58^{+0.08}_{-0.08}$	$0.56^{+0.08}_{-0.08}$	3874^{+283}_{-174}	$0.15^{+0.17}_{-0.17}$	1	30.4	15.78	13.48	12.64
5228	6036286	1	$0.37^{+0.07}_{-0.05}$	$0.36^{+0.06}_{-0.05}$	3434^{+72}_{-73}	$0.00^{+0.10}_{-0.10}$	2	53.6	15.35	12.77	11.94
5359	7130612	1	$0.55^{+0.05}_{-0.05}$	$0.53^{+0.05}_{-0.05}$	3939^{+52}_{-51}	$-0.20^{+0.10}_{-0.10}$	2	16.3	16.56	14.41	13.59
5692	9575728	1	$0.55^{+0.05}_{-0.06}$	$0.54^{+0.05}_{-0.05}$	3901^{+50}_{-95}	$-0.10^{+0.10}_{-0.10}$	2	39.8	14.14	12.00	11.18

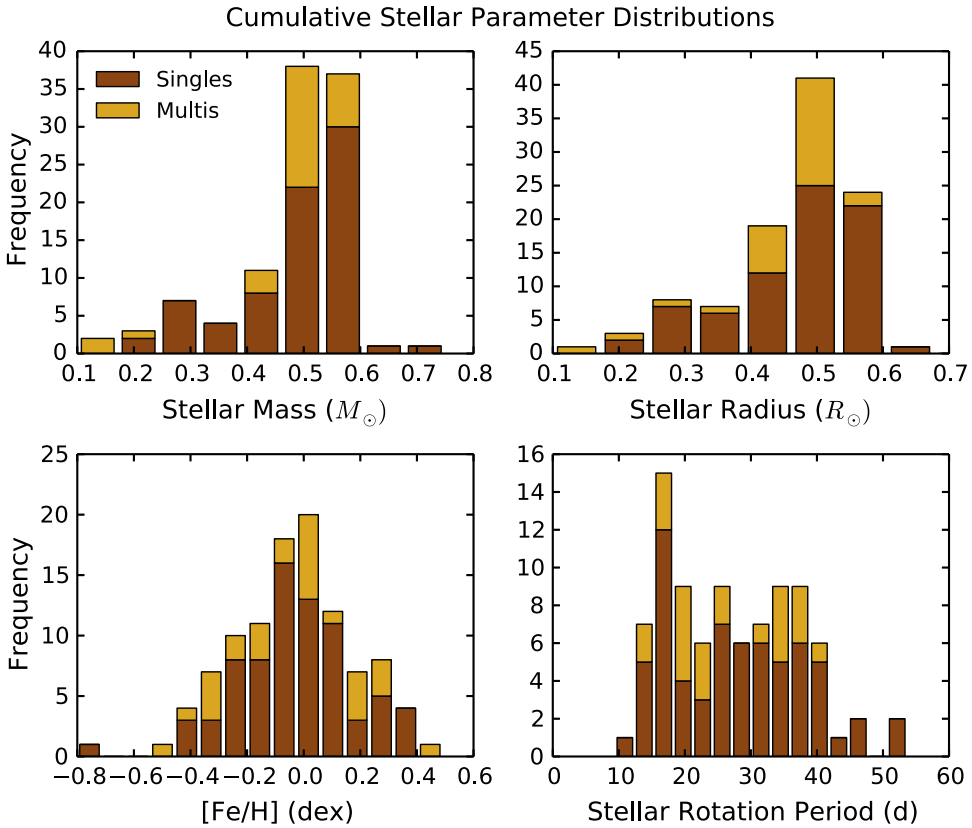

Figure 10. Distributions of stellar parameters for the final ensemble of 104 cool KOIs. The host stars of single transit systems and multi-transit systems have been distinguished and are shown in dark and light shading, respectively.

The cumulative distributions for the four transit parameters that are most relevant to the planet statistics are displayed in Figure 9. For this plot and those that follow, we distinguish between the planets that are in single transit and multi-transit systems.

6.1. Stellar Characteristics

The physical parameters of the transiting planets are intimately tied to the stellar parameters. We therefore also consolidate data for the stellar sample both from this work and from the literature. Stellar masses, radii, and effective temperatures were obtained from the lists of Muirhead et al. (2014) and Dressing & Charbonneau (2013). By default, we use the stellar parameters derived from the medium-resolution, infrared spectroscopy of Muirhead et al. (2014). The method uses a calibrated empirical relationship between the shape of the pseudo-continuum in the *K*-band spectrum to infer a stellar effective temperature (H_2O-K2 index; Rojas-Ayala et al. 2012). The equivalent widths of the Ca I triplet and Na I doublet within the same band are used to estimate the stellar metallicity using a relationship calibrated on nearby wide binaries with FGK type stars (Rojas-Ayala et al. 2010). The mass and radius of the star are then estimated by interpolating these $T_{\rm eff}$ and [M/H] values onto stellar evolutionary tracks (Dotter et al. 2008; Feiden et al. 2011).

For KOIs that do not have parameters derived with near-infrared spectra, we use the stellar parameters from Dressing & Charbonneau (2013). Here, the authors interpolate the wide band photometry from the KIC (Brown et al. 2011) onto stellar evolution models to obtain masses, radii, and metallicities. The mass and radius values derived by this method are typically in reasonable agreement with Muirhead et al. (2014), while the metallicity estimates are comparatively less reliable.

These compiled values and errors are presented in Table 5 along with the photometry from the KIC. In addition to this information, we also include our estimate of the stellar rotation period derived from the rotational modulation of an inhomogeneous surface brightness distribution. We are able to detect this rotational signature in a large fraction of our sample, about 86%, and report the period corresponding to the largest peak of the auto-correlation function that we validate by visual inspection. The stellar rotation period can be an important parameter in the characterization of the planet sample as this allows for age estimates (Barnes 2003) as well as activity levels (e.g., Reiners et al. 2012). The distribution of stellar parameters is shown for host stars of single and multi-transit systems in Figure 10.

7. SUMMARY AND CONCLUSION

Many exciting discoveries and insights from the *Kepler* Mission have come from the relatively small sample of M dwarf stars (Johnson et al. 2011b, 2012; Muirhead et al. 2012b, 2013; Dressing & Charbonneau 2013; Ballard & Johnson 2014; Kipping et al. 2014; Morton & Swift 2014; Quintana et al. 2014). The small sizes of these stars make it easier to probe deeper into the realm of super-Earth and terrestrial planets where planets form most readily. The cool surface temperatures facilitate detections of ever smaller planets in or near where liquid water may exist on their surfaces due to the shorter orbital periods and higher transit probability. While this sample is a mere 2% of the total number of stars *Kepler* observed during its primary mission, it offers a glimpse into the formation of the most numerous planets orbiting the most numerous stars in the Galaxy.

These facts have played a large role in motivating our group's efforts to understand this population of stars and planets. In this work, we present a uniform analysis of the photometry of cool dwarf stars spanning the full *Kepler* primary mission, the results of which are catalogs of transit parameters and stellar parameters for 163 transit candidates orbiting 104 low-mass dwarf stars. The stellar parameters are taken primarily from Muirhead et al. (2014) and are supplemented with values from Dressing & Charbonneau (2013). We add new stellar rotation periods estimated directly from the *Kepler* light curves, and recover rotational modulation for approximately 86% of our targets.

As the statistical treatments of the *Kepler* data set continue to advance and improve, these transit parameters are meant to serve as a valuable data set. To facilitate further studies, we provide the posterior distributions of the transit parameters for each planet candidate including short cadence fit parameters where available. Diagnostic plots for each KOI created during the reduction and analysis of the light curves are also available for each star and transit.

J.J.S. would like to thank Jason Eastman, David Kipping, Ellen Price, and Natalie Batalha for their helpful input regarding various aspects of this work. All of the data presented in this paper were obtained from the MAST. STScI is operated by the Association of Universities for Research in Astronomy, Inc., under NASA contract NAS5-26555. Support for MAST for non-*Hubble Space Telescope* data is provided by the NASA Office of Space Science via grant NNX13AC07G and by other grants and contracts. This paper includes data collected by the *Kepler* mission. Funding for the *Kepler* mission is provided by the NASA Science Mission directorate. A.V. and B.T.M. are supported by the National Science Foundation Graduate Research Fellowship, grant No. DGE 1144152 and DGE 1144469, respectively.

REFERENCES

Agol, E., Steffen, J., Sari, R., & Clarkson, W. 2005, MNRAS, 359, 567
Akeson, R. L., Chen, X., Ciardi, D., et al. 2013, PASP, 125, 989
Ballard, S., & Johnson, J. A. 2014, arXiv:1410.4192
Barnes, S. A. 2003, ApJ, 586, 464
Batalha, N. M., Rowe, J. F., Bryson, S. T., et al. 2013, ApJS, 204, 24
Batygin, K., & Morbidelli, A. 2013, AJ, 145, 1
Borucki, W. J., Koch, D., Basri, G., et al. 2010, Sci, 327, 977
Borucki, W. J., Koch, D. G., Basri, G., et al. 2011a, ApJ, 728, 117
Borucki, W. J., Koch, D. G., Basri, G., et al. 2011b, ApJ, 736, 19
Brown, T. M., Latham, D. W., Everett, M. E., & Esquerdo, G. A. 2011, AJ, 142, 112
Burke, C. J., Bryson, S. T., Mullally, F., et al. 2014, ApJS, 210, 19
Carter, J. A., & Winn, J. N. 2009, ApJ, 704, 51
Chiang, E., & Laughlin, G. 2013, MNRAS, 431, 3444
Christiansen, J. L., Clarke, B. D., Burke, C. J., et al. 2013, ApJS, 207, 35
Coughlin, J. L., Thompson, S. E., Bryson, S. T., et al. 2014, AJ, 147, 119
Dotter, A., Chaboyer, B., Jevremović, D., et al. 2008, ApJS, 178, 89
Dressing, C. D., & Charbonneau, D. 2013, ApJ, 767, 95
Fabrycky, D. C., Ford, E. B., Steffen, J. H., et al. 2012, ApJ, 750, 114
Fabrycky, D. C., Lissauer, J. J., Ragozzine, D., et al. 2014, ApJ, 790, 146
Fang, J., & Margot, J.-L. 2012, ApJ, 761, 92
Feiden, G. A., Chaboyer, B., & Dotter, A. 2011, ApJL, 740, L25
Fischer, D. A., Schwamb, M. E., Schawinski, K., et al. 2012, MNRAS, 419, 2900
Ford, E. B., Rowe, J. F., Fabrycky, D. C., et al. 2011, ApJS, 197, 2
Foreman-Mackey, D., Hogg, D. W., Lang, D., & Goodman, J. 2013, PASP, 125, 306

Foreman-Mackey, D., Hogg, D. W., & Morton, T. D. 2014, ApJ, 795, 64
Fressin, F., Torres, G., Charbonneau, D., et al. 2013, ApJ, 766, 81
Goldreich, P., & Schlichting, H. E. 2014, AJ, 147, 32
Hansen, B. M. S., & Murray, N. 2012, ApJ, 751, 158
Henry, T. J., Kirkpatrick, J. D., & Simons, D. A. 1994, AJ, 108, 1437
Henry, T. J., Subasavage, J. P., Brown, M. A., et al. 2004, AJ, 128, 2460
Holman, M. J., & Murray, N. W. 2005, Sci, 307, 1288
Howard, A. W., Marcy, G. W., Bryson, S. T., et al. ApJS, 201, 15
Jenkins, J. M., Caldwell, D. A., Chandrasekaran, H., et al. 2010, ApJL, 713, L87
Johnson, J. A., Apps, K., Gazak, J. Z., et al. 2011, ApJ, 730, 79
Johnson, J. A., Gazak, J. Z., Apps, K., et al. 2012, AJ, 143, 111
Kipping, D. M. 2010a, MNRAS, 408, 1758
Kipping, D. M. 2010b, MNRAS, 407, 301
Kipping, D. M. 2013, MNRAS, 435, 2152
Kipping, D. M., Nesvorný, D., Buchhave, L. A., et al. 2014, ApJ, 784, 28
Koch, D. G., Borucki, W. J., Basri, G., et al. 2010, ApJL, 713, L79
Kovács, G., Zucker, S., & Mazeh, T. 2002, A&A, 391, 369
Lissauer, J. J., Fabrycky, D. C., Ford, E. B., et al. 2011a, Natur, 470, 53
Lissauer, J. J., Marcy, G. W., Bryson, S. T., et al. 2014, ApJ, 784, 44
Lissauer, J. J., Ragozzine, D., Fabrycky, D. C., et al. 2011b, ApJS, 197, 8
Lithwick, Y., & Wu, Y. 2012, ApJL, 756, L11
Mandel, K., & Agol, E. 2002, ApJL, 580, L171
Mann, A. W., Gaidos, E., & Ansdell, M. 2013, ApJ, 779, 188
Mann, A. W., Gaidos, E., Lépine, S., & Hilton, E. J. 2012, ApJ, 753, 90
Markwardt, C. B. 2009, in ASP Conf. Ser. 411, Astronomical Data Analysis Software and Systems XVIII, ed. D. A. Bohlender, D. Durand, & P. Dowler (San Francisco, CA: ASP), 251
Mazeh, T., Nachmani, G., Holczer, T., et al. 2013, ApJS, 208, 16
Morton, T. D. 2012, ApJ, 761, 6
Morton, T. D., & Johnson, J. A. 2011, ApJ, 738, 170
Morton, T. D., & Swift, J. 2014, ApJ, 791, 10
Muirhead, P. S., Becker, J., Feiden, G. A., et al. 2014, ApJS, 213, 5
Muirhead, P. S., Hamren, K., Schlawin, E., et al. 2012a, ApJL, 750, L37
Muirhead, P. S., Johnson, J. A., & Apps, K. 2012b, ApJ, 747, 144
Muirhead, P. S., Mann, A. W., Vanderburg, A., et al. 2015, arXiv
Muirhead, P. S., Vanderburg, A., Shporer, A., et al. 2013, ApJ, 767, 111
Mullally, F., Coughlin, J. L., Thompson, S. E., et al. 2015, ApJS, 217, 31
Newton, E. R., Charbonneau, D., Irwin, J., & Mann, A. W. 2015, ApJ, 800, 85
Ofir, A. 2014, A&A, 561, A138
Ofir, A., & Dreizler, S. 2013, A&A, 555, A58
Petigura, E. A., Howard, A. W., & Marcy, G. W. 2013a, PNAS, 110, 19273
Petigura, E. A., Marcy, G. W., & Howard, A. W. 2013b, ApJ, 770, 69
Pont, F., Zucker, S., & Queloz, D. 2006, MNRAS, 373, 231
Price, E. M., & Rogers, L. A. 2014, ApJ, 794, 92
Quintana, E. V., Barclay, T., Raymond, S. N., et al. 2014, Sci, 344, 277
Reid, I. N., & Cruz, K. L. 2002, AJ, 123, 2806
Rein, H. 2012, MNRAS, 427, L21
Reiners, A., Joshi, N., & Goldman, B. 2012, AJ, 143, 93
Rodríguez-López, C., MacDonald, J., & Moya, A. 2012, MNRAS, 419, L44
Rojas-Ayala, B., Covey, K. R., Muirhead, P. S., & Lloyd, J. P. 2010, ApJL, 720, L113
Rojas-Ayala, B., Covey, K. R., Muirhead, P. S., & Lloyd, J. P. 2012, ApJ, 748, 93
Rowe, J. F., Bryson, S. T., Marcy, G. W., et al. 2014, ApJ, 784, 45
Rowe, J. F., Coughlin, J. L., Antoci, V., et al. 2015, ApJS, 217, 16
Sanchis-Ojeda, R., Rappaport, S., Winn, J. N., et al. 2014, ApJ, 787, 47
Schlichting, H. E. 2014, ApJL, 795, L15
Seager, S., & Mallén-Ornelas, G. 2003, ApJ, 585, 1038
Smith, J. C., Stumpe, M. C., van Cleve, J. E., et al. 2012, PASP, 124, 1000
Steffen, J. H., Fabrycky, D. C., Agol, E., et al. 2013, MNRAS, 428, 1077
Stumpe, M. C., Smith, J. C., van Cleve, J. E., et al. 2012, PASP, 124, 985
Swift, J. J., Johnson, J. A., Morton, T. D., et al. 2013, ApJ, 764, 105
Szabó, R., Szabó, G. M., Dálya, G., et al. 2013, A&A, 553, A17
Tremaine, S., & Dong, S. 2012, AJ, 143, 94
Winn, J. N., Holman, M. J., Torres, G., et al. 2008, ApJ, 683, 1076
Wu, H., Twicken, J. D., Tenenbaum, P., et al. 2010, Proc. SPIE, 7740, 19
Wu, Y., & Lithwick, Y. 2013, ApJ, 772, 74